Charles University in Prague
Faculty of Mathematics and Physics

MASTER THESIS

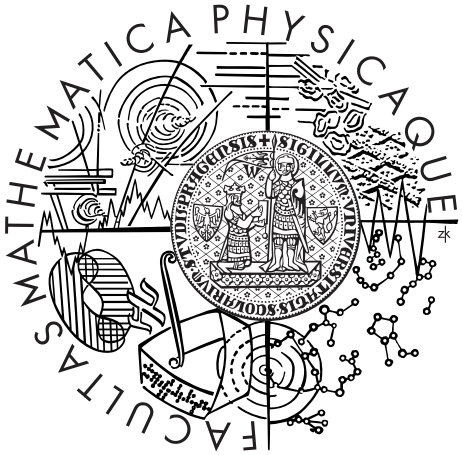

Jiří Vackář

Fast interference waves and 1D seismic crustal models

Department of Geophysics

Supervisor of the master thesis: prof. RNDr. Jiří Zahradník DrSc.
Study programme: Physics
Specialization: Geophysics

Prague 2012

Acknowledgements

First of all, I would like to thank prof. Jiří Zahradník, for his excellent pedagogical approach. He has always willing to help me with emerging problems, to discuss them and give me useful advice. I am grateful for his patient reading this thesis many times and correcting both my English writing so as other mistakes.

Further, I would like to thank Oldřich Novotný for for his great help with theoretical dispersion curves, Petr Kolínský who introduced me to using his program SVAL, Vladimír Plicka for useful code for solving inversion problem, Jaromír Janský for explanation of calculating travel times and using program HYPO and Jan Linek for language corrections. I also express my thank to all members of Department of Geophysics for the friendly and inspiring atmosphere they created.

Last but not least I thank to my parents for their support all the time I have studied.

The work was supported by the grants SVV-2012-265308 and GAČR 210/11/0854.

I declare that I carried out this master thesis independently, and only with the cited sources, literature and other professional sources.

I understand that my work relates to the rights and obligations under the Act No. 121/2000 Coll., the Copyright Act, as amended, in particular the fact that the Charles University in Prague has the right to conclude a license agreement on the use of this work as a school work pursuant to Section 60 paragraph 1 of the Copyright Act.

Prague, April 13, 2012 Jiří Vackář

Název práce: Rychlé interferenční vlny a 1D seismické modely kůry

Autor: Jiří Vackář

Katedra: Katedra geofyziky

Vedoucí diplomové práce: prof. RNDr. Jiří Zahradník DrSc.

Abstrakt: Při nedávném mělkém zemětřesení v Korintském zálivu v Řecku (M_w 5,3) byly pozorovány neobvyklé dlouhoperiodické vlny (periody 5 sekund a více). Zaznamenány byly na několika regionálních stanicích mezi příchodem P- a S-vlny. Pětisekundová perioda je mnohem delší než trvání zdroje a ukazuje na efekt struktury. Pozorované seismogramy byly zkoumány metodami frekvenčně-časové analýzy. Určené disperzní křivky rychlé dlouhoperiodické vlny měly grupové rychlosti od 3 do 5,5 km/s pro periody v rozsahu 4–10 s, s velkými rozdíly mezi stanicemi. Zobecněná disperzní křivka se rozděluje do dvou hlavních pásů, pravděpodobně spojených s laterálními variacemi zemské kůry. Řešením přímé úlohy pro více existujících modelů kůry a jejich modifikací jsme provedli analýzu citlivosti, která ukázala, že zkoumaná vlna je ovlivněna zejména nízkorychlostními vrstvami v nejsvrchnějších cca 4 kilometrech kůry. Závěrem jsme získali model mělké kůry inverzí seismogramů pomocí algoritmu nejbližší soused. Inverze potvrdila, že zkoumanou vlnu je možné vysvětlit 1-D modelem kůry, ale ne na více stanicích najednou. Modely závislé na dráze šíření představují částečné vysvětlení pro pásy tvořené pozorovanými disperzními křivkami. Jinou alternativou je příspěvek několika tzv. prosakujících módů.

Klíčová slova: interferenční vlna, rychlá dlouhoperiodická vlna, disperzní křivka, inverze kůry, prosakující módy

Title: Fast interference waves and 1D seismic crustal models

Author: Jiří Vackář

Department: Department of Geophysics

Supervisor: prof. RNDr. Jiří Zahradník DrSc.

Abstract: A recent shallow earthquake in the Corinth Gulf, Greece (M_w 5.3) generated unusual long-period waves (periods $>$ 5 seconds) between the P- and S-wave arrival. The 5-second period, being significantly longer than the source duration, indicates a structural effect. Observed seismograms were examined by methods of the frequency-time analysis. Dispersion curves of the fast long-period (FLP) waves indicated group velocities ranging from 3 to 5.5 km/s for periods between 4 and 10 s, respectively, with large variations among the stations. The generalized dispersion curve splits into two major strips, probably related to lateral variations of the crustal structure. Forward simulations for several existing crustal models were made. A few partially successful models served for a sensitivity study, which showed that the FLP wave seemed to be mainly due to the low-velocity layers in the uppermost 4 kilometers of the crust. Finally the shallow crustal structure was retrieved by inverting observed seismograms by Neighborhood algorithm. The inversion confirmed that the FLP wave in seismograms at more than a single station cannot be explained with a 1-D crustal model. The path-dependent models provided a partial explanation for the strips revealed in the experimental dispersion curves. An alternative explanation is by contribution of several leaking modes.

Keywords: interference wave, fast long-period wave, dispersion curve, crustal inversion, leaking modes

Contents

Introduction

Seismic records of shallow near-regional earthquakes recorded at stations in Greece are usually very complicated. In particular, S-wave onset is often obscured by P-wave coda. This thesis is devoted to another complexity of the records – i.e. the occurrence of unusual fast long period (FLP) wave between P- and S-wave onset. The wave was first recognized in relation to our investigation of the Efpalio 2010 earthquake sequence (Sokos *et al.*, 2012). The FLP-wave predominant periods ranged from 5 to 8 seconds, the wave was observed at stations in the epicentral distance from $\sim$ 30 to $\sim$ 230 km. The 5-second period, being significantly longer than the source duration, indicates a structural effect.

The observed wave has some characteristic features similar to the PL wave, broadly investigated in the 60s–70s. Dainty (1971) presented a theory of leaking modes in a multilayered elastic half-space, which explains oscillatory arrivals between P and S on seismograms. In contrast to real-valued roots of the dispersion equation in simple 1D media, corresponding to the standard higher modes of surface waves, the leaking modes were related to complex roots. Oliver (1961) explained observation of several earthquakes in terms of coupling between the incident shear waves and leaking modes, especially lowest leaking mode, the PL wave. Oliver and Major (1960) reported that PL waves correspond to leaking mode propagation within near-surface wave guide and showed dispersion curves of PL waves for several earthquakes. Su and Dorman (1965) described some properties of leaking modes and related them to continental wave-guide. All of these studies focus on earthquakes at distances of thousands of kilometers and periods of tens of seconds, in contrast to our observations in relatively short distances and shorter periods. We do not know any study of leaking modes at near-regional distances. We also do not know any study devoted to modeling the observed leaking modes by synthesis of complete seismograms

Another well-known fast long period wave is the W phase, which can be used for rapid source parameters determination and tsunami warning. This wave is usually explained as superposition of the fundamental, first, second and third overtones of spheroidal modes or Rayleigh waves and has period range of 100–1000 s (Kanamori and Rivera, 2008).

Therefore, the basic question is "what kind of wave is the FLP wave?". It is possible that the FLP-wave is of the same nature as PL or W, but in much smaller scale. The question about the origin and nature of the FLP wave is not only 'academic'. Having some special properties, the wave might perhaps provide some independent constraints for the crustal-structure and seismic-source investigations. We aim at answering the basic question, but also at using the FLP to partially improve the existing seismic crustal models.

The thesis is structured as follows. In Chapter 1 we briefly describe our observation about FLP-wave in order to define its basic properties, such as predominant periods, epicentral and azimuthal dependence of its strength, as well as its occurrence on different components of the record. We continue in Chapter 2 by description of methods and software used: the Discrete wavenumber method (synthetic seismograms), SVAL (frequency-time analysis) and VDISP (theoretical dispersion curves). Then we describe synthetic tests to define practical limits

of the frequency-time analysis. In Chapter 3, we start with investigation of observed records by methods of dispersion analysis. It ends with slightly pessimistic finding that the dispersion curves are not always reliable, and we are not always able to calculate theoretical curves matching the observed ones. Therefore, in next parts, we focus directly on seismograms, without the intermediate step via dispersion curves. In Chapter 4, we search for parameters of the crust, most strongly affecting the occurrence of the FLP wave. The sensitivity is studied by comparing real seismograms with synthetic ones for several existing crustal models of the studied region, and/or by altering some of the parameters of the structural models. The results of the sensitivity analysis are used to suitably formulate (and parametrize) an inverse problem in which complete seismograms are used to retrieve the uppermost part of the crust (down to the 4-km depth) by the Neighborhood algorithm (Chapter 5). Properties of the best-fitting models and uncertainty of model parameters are discussed. Finally, in Chapter 6, we return to dispersion curves, analyze them for the best-fitting models, and look for their physical interpretation in terms of leaking modes.

1. Observation

1.1 Efpalio 2010 earthquake

The Efpalio 2010 earthquake sequence occurred in the western part of the Gulf of Corinth, Greece. This region is tectonically complicated, with many faults and complex geological structure (Latorre *et al.*, 2004). The strongest events of the sequence were two earthquakes with magnitude greater than 5, both exhibiting normal faulting along E–W trending planes (Sokos *et al.*, 2012). In this thesis we will study the strongest event, the January 18, 2010 earthquake. Its parameters are presented in Table 1.1.

origin time	January 18, 2010 15:56 UTC
hypocenter	38.419° N, 21.915° E
	depth 6.6 km
centroid	38.422° N, 21.941° E
	depth 4.5 km
seismic moment	$0.97 \cdot 10^{17}$ Nm
moment magnitude M_w	5.3

Table 1.1: Parameters of the Efpalio earthquake according to Sokos *et al.* (2012).

1.2 Seismic stations and data used

We have inspected data from 21 seismic stations, where the Efpalio earthquake was recorded (see Fig. 1.1). The stations are equipped with broad-band seismometers, mostly Guralp CMG-3T and Trillium 40. The records were instrumentally-corrected and re-sampled with frequency 33 Hz.

We excluded three stations with the smallest epicentral distances (less then 20 km), because their records differ qualitatively from the others; so finally we study data from 18 stations.

1.3 Basic findings

The Efpalio 2010 earthquake records are relatively complicated, it is difficult to say which part of the record corresponds to what phase. A noticeable long-period wave (with period 4–8 seconds) was observed at some stations in the initial part of the record, in the interval between the *P*- and *S*-wave arrival (Fig. 1.2).

After rotating the records into R, T, Z system by means of station azimuth determined from location we found that the fast long-period wave (hereafter also FLP-wave, for simplicity) is strong on the radial and vertical component, but weak or absent on the transversal component (Fig. 1.3).

Another basic observation is that in a considerable number of the stations the FLP-wave is significant, having its amplitude of the same order as the seismogram maximum in the surface-wave group (Fig. 1.4). At some other stations, the wave is present, but much weaker (Fig. 1.5). There are a few stations where the wave

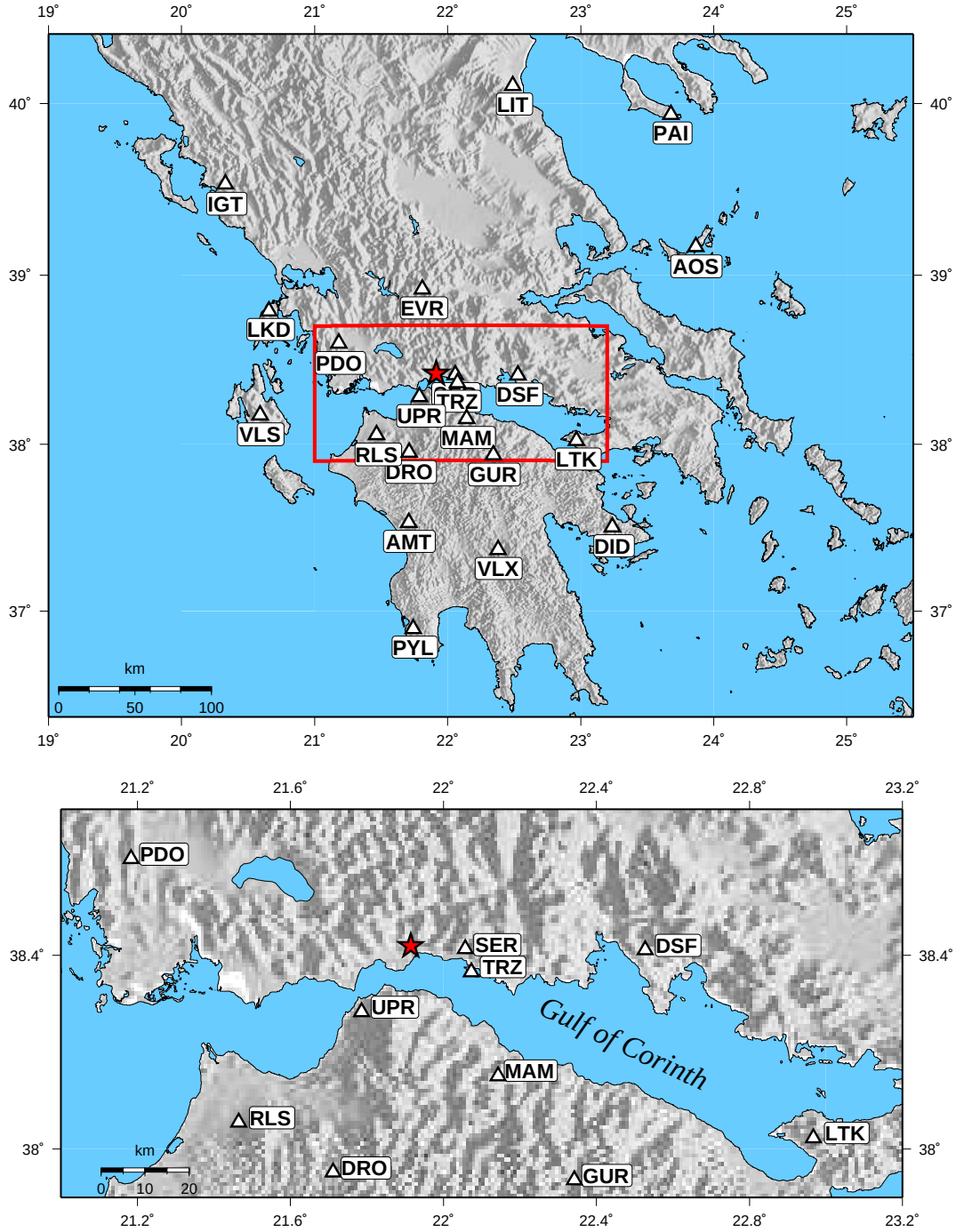

Figure 1.1: Map of the studied part of Greece (top) with a rectangle showing the epicentral region in detail (bottom). Epicenter of the Efpalio earthquake is labeled by a red star. The stations used in the study are labeled by triangles.

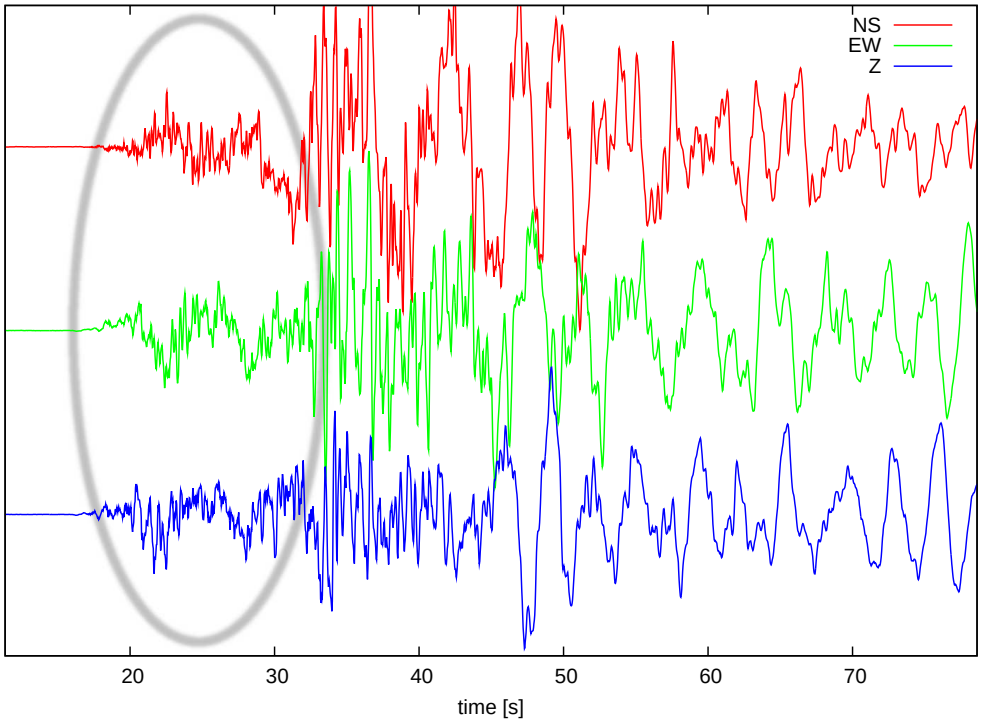

Figure 1.2: Instrumentally corrected three-component (NS, EW, Z) velocity record from station LTK (Loutraki, epicentral distance 102 km). A fast long-period wave (of about 5-second period) is significant on all three components.

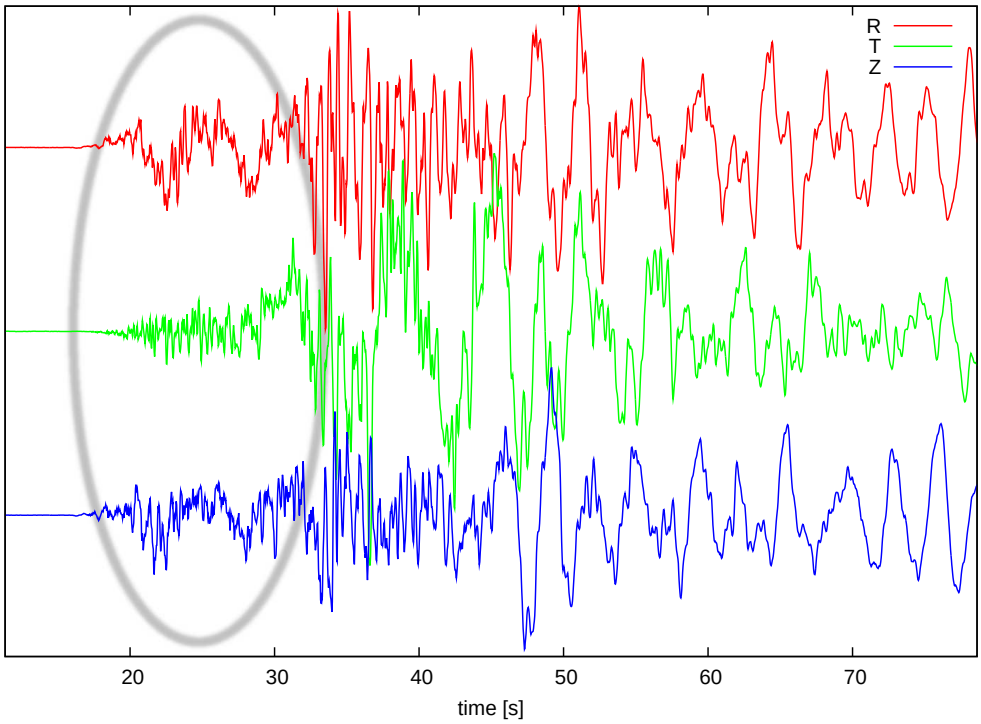

Figure 1.3: Velocity record as in Fig. 1.2, rotated into R, T, Z components. The long-period wave is observable only on the radial (red) and vertical (blue) component. On the transversal component (green) this wave is weak or absent.

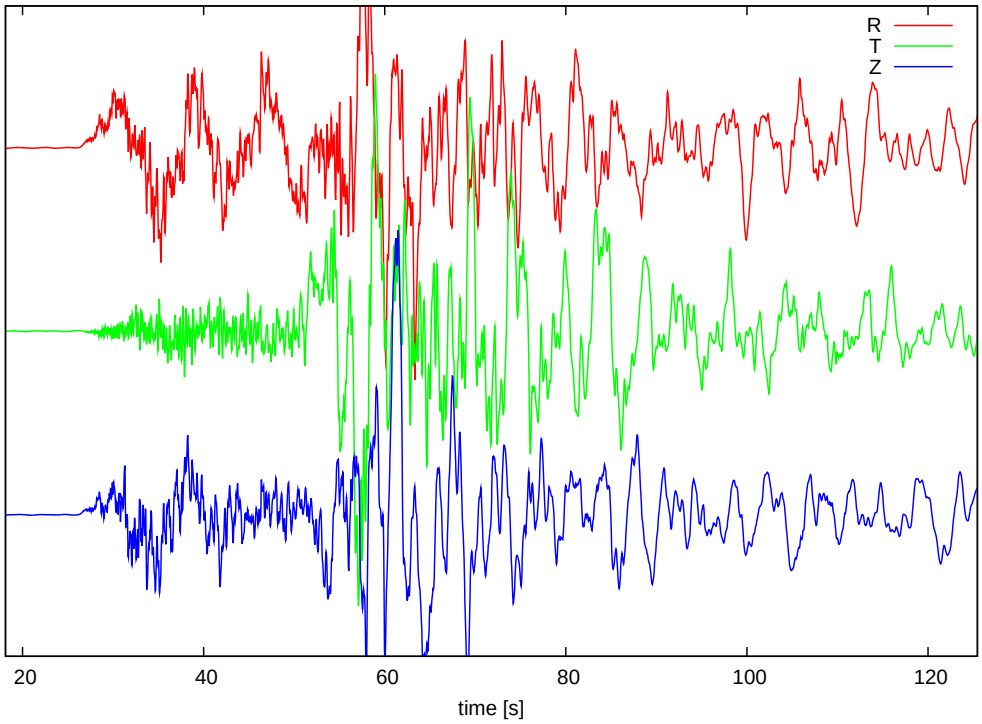

Figure 1.4: Instrumentally corrected, rotated velocity record of the Efpalio 2010 earthquake on broad-band station PYL (Pylos, epicentral distance 170 km). There is a strong FLP-wave on the radial and vertical component with prevailing period of about 8 seconds, starting with *P*-wave arrival.

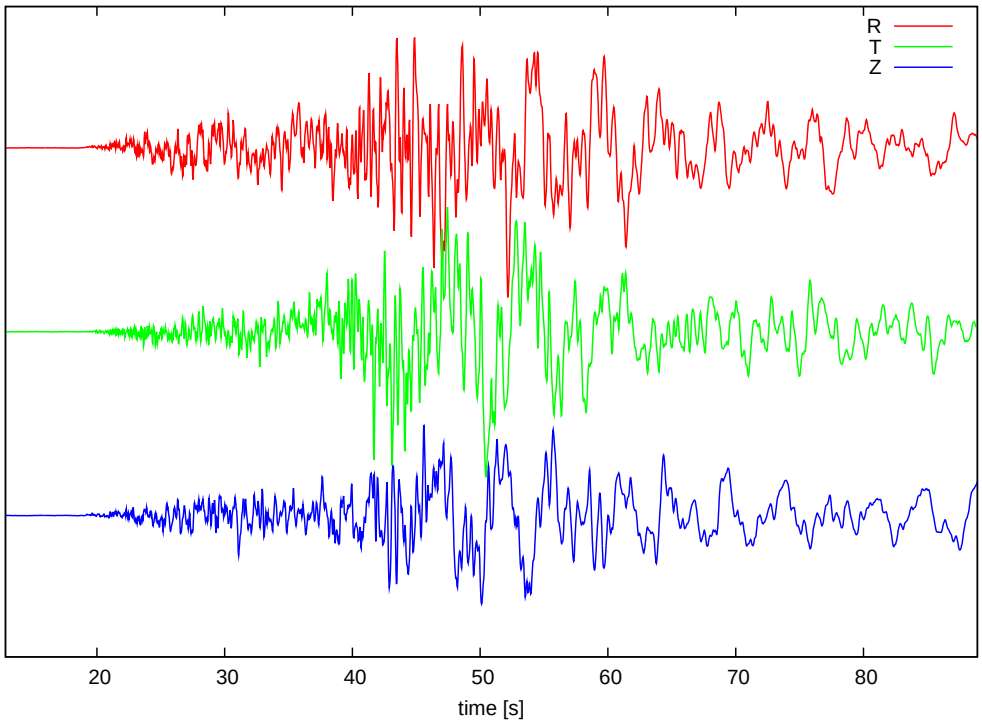

Figure 1.5: Instrumentally corrected, rotated velocity record of the Efpalio 2010 earthquake on broad-band station LKD (Lefkada, epicentral distance 117 km). A fast long-period wave is much weaker than in Figs 1.3 and 1.4.

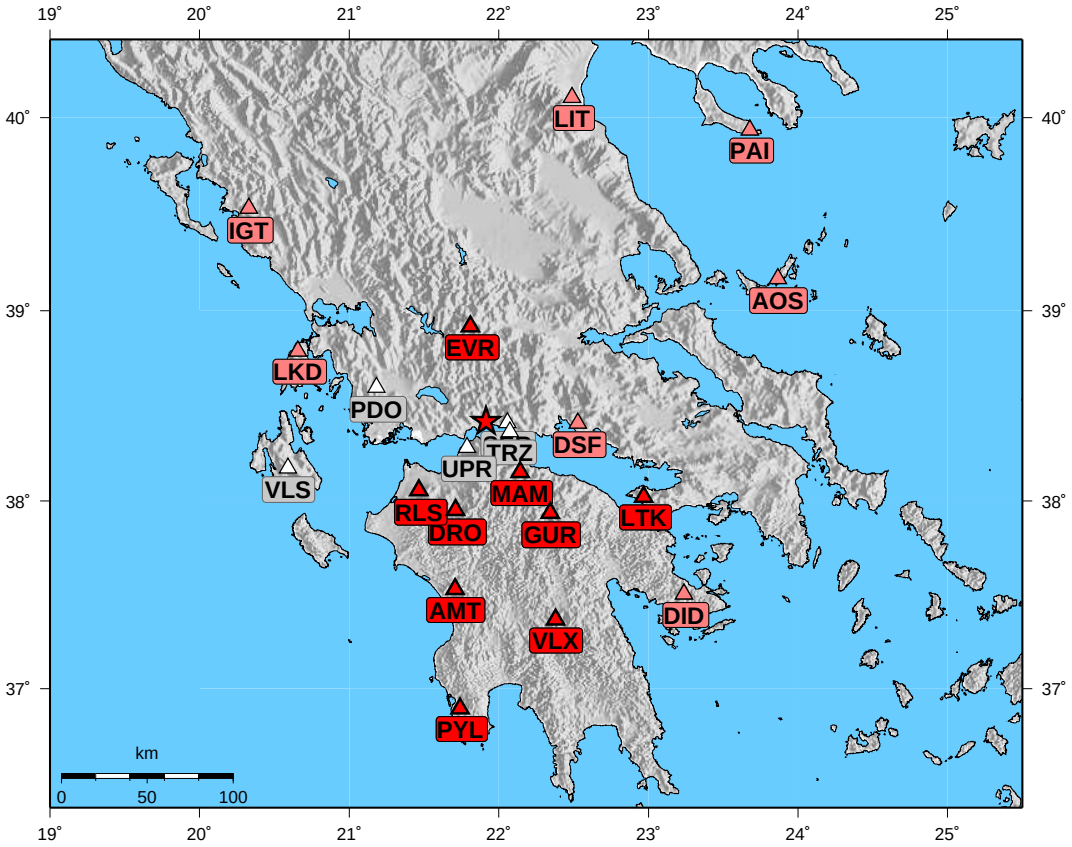

Figure 1.6: The stations are marked according to the strength of the observed long-period wave: strong – dark red, weak – light red, absent – white. The classification is based on the ratio between the amplitudes of the FLP-wave and the strongest wave group in the record (surface waves); the strong, weak, and absent FLP-waves refers to the ratio of about 20–50 %, 5–15 % and less than 5 %, respectively.

is visually not apparent. As observed in the map (see Fig. 1.6), the FLP-wave occurrence has no simple dependence on azimuth and epicentral distance. It seems that the FLP-wave is weak or absent on islands, but there are probably more factors which influence its occurrence and strength.

2. Methods and computer programs used

In this chapter we describe computer programs and methods of seismogram analysis, which we use in the next chapters for dispersion analysis and sensitivity study. We also perform some synthetic tests to recognize practical limits of the methods.

We focus on fundamental mode of the Rayleigh wave instead of the FLP-wave in some of the tests. The Rayleigh wave study is simpler and it allows us to prepare for the study of the FLP-wave; in particular, we will be able to compare the experimentally derived dispersion curve with the analytically derived one. The fundamental mode is also the strongest wave group in the most of synthetic seismograms, so there is no problem with finding it by the dispersion analysis.

2.1 Discrete wavenumber method

Synthetic seismograms in this thesis are calculated by the *Discrete wavenumber method* (hereafter referred as DW method), introduced by Bouchon (1981). Here we present a short overview of the method.

Green's function for a 1-D structure can be expressed as a double integral over frequency and wavenumber. The wavenumber integral can be exactly expressed by a discrete summation if a single source is formally substituted by sources periodically distributed in space. Specifically, it may be achieved by a grid of sources in the plane defined by horizontal components of wavenumbers k_x and k_y or by a set of sources distributed along circles centered at the studied point source, i.e. the sources distributed at equal radial interval if using cylindrical coordinate system with radial wavenumber k. The periodicity interval must be chosen such that disturbance from the periodically repeating sources arrive after time interval of interest. The periodic sources are further reduced by artificial attenuation.

The method combines the analytic solution for a homogeneous isotropic unbounded medium with matrix method of wave field calculation in a layered medium introduced by Kennett and Kerry (1979).

To facilitate the numerical experiments, a special interface code has been developed in this thesis. The interface performs batch processing of programs for generation of synthetic seismograms, i.e. Green's function calculation, and their convolution with the source time function.

It should be run with one or more parameters. The first parameter (required) is name of directory where the results will be saved, and where input files with description of the crust, source and some technical parameters may be placed. None of that input files is necessary – files that are not present are replaced by default setting. The other parameters might change the regime of the computation – e. g. calculate seismograms using previously determined Green's function, use another time function instead of the default one, and compute the displacement instead of the velocity.

Many output files are produced, and they are arranged into hierarchical directory structure. There are seismograms both in N, E, Z and R, T, Z system, written in two file formats: 4-column ASCII format without header suitable for plotting, and the so-called KUK ASCII file dedicated for the SVAL program. The seismograms are also automatically plotted in more variants – three component of each station in one figure with automatically determined amplitude, the same figure with fixed amplitude related to the amplitude of the related real record (useful for comparison in the absolute value) and radial components of all stations in one figure for overview.

The developed interface makes it possible to calculate synthetic seismograms for many crustal models and different source parameters more efficiently than when repeatedly executing several programs and organizing results manually. Technically, the interface was programmed in bash language, with plotting in gnuplot.

2.1.1 Verification ot the method

We perform a simple verification of the code, the interface and their proper usage. Bouchon (1981) showed a simple example of the DW calculation (an explosion in the halfspace observed on the surface). We calculated the same case and arrived to the same result (Fig. 2.1).

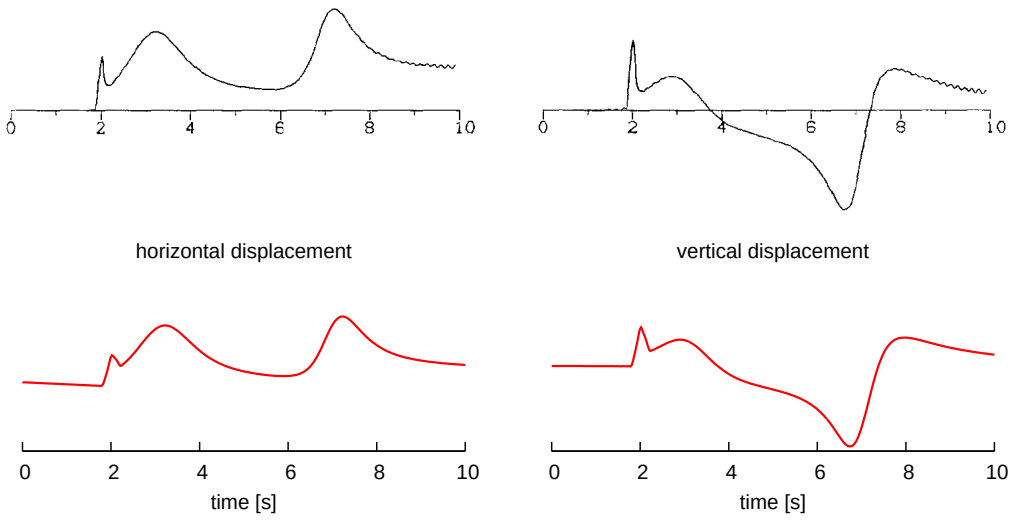

Figure 2.1: Test of the syntetic seismogram calculation. Figure reprinted from Bouchon (1981) (top) compared to our computation with the same parameters (bottom).

2.2 Frequency-time analysis of records

Frequency-time analysis is a methods to simultaneously inspect the spectral content of the signal and its temporal variation. In this section we will focus on the

multiple filtering method, representing one of possible modes of the frequency-time analysis. The description and terminology is adopted from Kolínský (2010).

2.2.1 Method

Let's introduce the multiple filtering method as an inverse Fourier transform

$$S(F,T) = \int_{-\infty}^{\infty} G(f)K(F,T,f)e^{2\pi ifT}df \ ; \tag{2.1}$$

where $S(F,T)$ is complex frequency-time representation of a signal, $G(f)$ is Fourier spectrum corresponding to the signal $g(t)$ in the time domain (earthquake record in our case) and $K(F,T,f)$ is a complex kernel. We use the notation that t is the variable of the time signal $g(t)$ and symbol T denotes the time variable of the resultant frequency-time representation $S(F,T)$. Analogously, symbol F denotes the frequency variable of $S(F,T)$ while symbol f is the variable of the Fourier spectrum $G(f)$.

If the kernel does not depend on T

$$K(F,T,f) = W(f,F) \ , \tag{2.2}$$

we can write (2.1) as

$$S(F,t) = \int_{-\infty}^{\infty} G(f)W(f,F)e^{2\pi ift}df \ . \tag{2.3}$$

The $W(f,F)$ is called weighting function with central frequency F.

We define the spectrogram as

$$P(F,t) = |S(F,t)|^2 \ . \tag{2.4}$$

The spectrogram $P(F,t)$ has the simple physical meaning – distribution of energy of signal both in time and frequency domain.

The key parameter for the analysis is the shape and width of the filters. We apply the Gaussian filters on spectrum in frequency domain. For a good resolution both at low and high frequencies, we use "the constant relative resolution filtering" defined as

$$W(f,F) = e^{\alpha(F)\frac{(f-F)^2}{F^2}} \ , \tag{2.5}$$

where parameter α controls the width of the filter. This parameter may, in general, vary with frequency. We use a linear function given by

$$\alpha(F) = a + b\frac{1}{F} \ . \tag{2.6}$$

In the SVAL program, described in the next subsection, there are parameters a and b implemented as variables which might be set by user.

2.2.2 SVAL program

The SVAL program, developed by Petr Kolínský, is an interactive software for frequency-time analysis. It may analyze dispersive signal of any frequency and dynamic range. It has also some other features, which we only briefly mention (see Kolínský (2010) for more detail) – e.g. inversion of measured dispersion curve into 1-D velocity structure and batch processing of many records. It uses the multiple filtering method.

In principle, the program enables to estimate the dispersion curve of any wave group in the record. Dispersion curve can be selected manually or by automatic procedure. The wave group corresponding to the chosen dispersion curve can be extracted.

Many parameters of the analysis may be entered and the result immediately checked in graphical tool, where all steps of the computation are displayed (Fig. 2.2). It is possible to easily repeat analysis with different parameters to find out a way of filtration and dispersion curve selection which gives reliable result.

Two file formats of input data are supported (one-column plain ASCII file and the SVAL own format – three column ASCII file with simple header).

The program is written in PASCAL using Borland Delphi environment. The SVAL program may be executed using one .exe file, it is compiled for Microsoft Windows. It does not require any installation or any other file present. It is a freeware available at author's web page: `http://www.irsm.cas.cz/~kolinsky/`

A small demonstration of the program is in Fig. 2.3 where there are different choices of the dispersion curve and resultant wave groups selected from the record.

2.2.3 Comparison of analysis in velocity and displacement

It was theoretically proved in the paper by Kolínský (2010) that the dispersion analysis of the velocity and displacement records gives the same result. We made an empirical verification by comparing the dispersion analysis of a velocity record and exactly same analysis of the corresponding displacement record (created by numeric integration using SeisGram2K software by Anthony Lomax). The obtained dispersion curves are not identical (see Fig. 2.4), but the difference is small in terms of the group-velocity scale of our data, and might be explained by a numeric inaccuracy.

2.3 Theoretical dispersion curve

There are two ways how to derive dispersion curves of waves propagating in a layered model. The first possibility is to generate synthetic seismograms, analyze them by the SVAL program and get the dispersion curve. It should be independent on azimuth, epicentral distance and source depth and parameters. If the wave is present at more than one component (e.g. Rayleigh wave on radial and vertical one), it should be also independent on component analyzed. Theoretically, any wave may be analyzed, but in practice the wave is required not to be very weak and not to be overlapped with any different wave.

Alternatively, for theoretically described waves, the analytic solution may be derived. We used this approach for validation of the first method in a special case

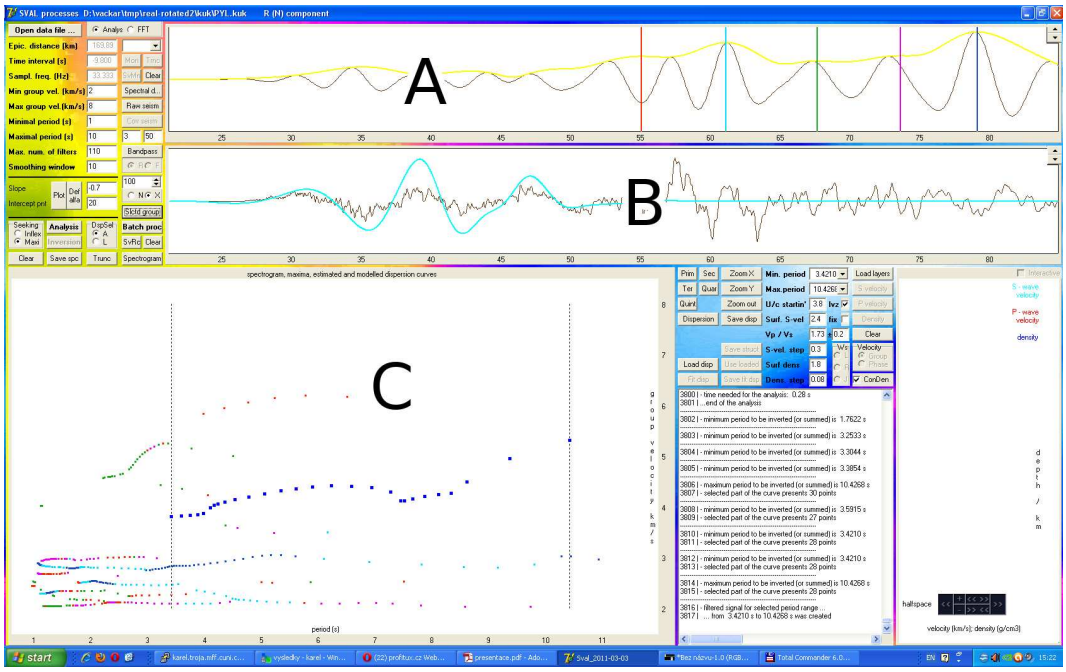

Figure 2.2: Screenshot of SVAL program (Kolínský, 2010). Panel labeled "A" shows the analyzed seismogram passed through one of the filters; the vertical lines at maxima of the envelope of filtered record correspond to the individual dispersion curves. Panel "B": The analyzed seismogram (gray) and the seismogram for the selected dispersion curve (azure). Panel "C": The spectrogram (period on horizontal axis, group velocity on vertical axis, color points representing the dispersion curves). Compared to the original SVAL output, colors of the panels were inverted here for better visibility of the printed version.

of the fundamental mode of Rayleigh wave and also in Chapter 6 while looking for theoretical interpretation of the FLP-wave.

We used program VDISP (version 1999) by Oldřich Novotný for calculation of theoretical dispersion curves. It allows computing dispersion curves of phase and group velocities and amplitude response of surface waves in a horizontally layered medium. It is based on matrix method using modified Thomson-Haskell matrices for Love waves and modified Watson's matrices for Rayleigh waves (Proskuryakova *et al.*, 1981).

2.4 'Experimental' vs. theoretical dispersion curves

We make a synthetic test to recognize practical limits of the SVAL program. The synthetic data were generated by the DW method for the same stations and parameters as in the real case of the Efpalio earthquake (Table 1.1). Crustal model *Novotny-LA3* (described later in section 4.1) was used.

The synthetic seismograms were rotated into R, T, Z system, and then analyzed by SVAL program. The analysis was performed on vertical component for all stations and on radial component for selected ones. The intention was to select a 'ridge' of the spectrogram obtained in SVAL program, which is related to the

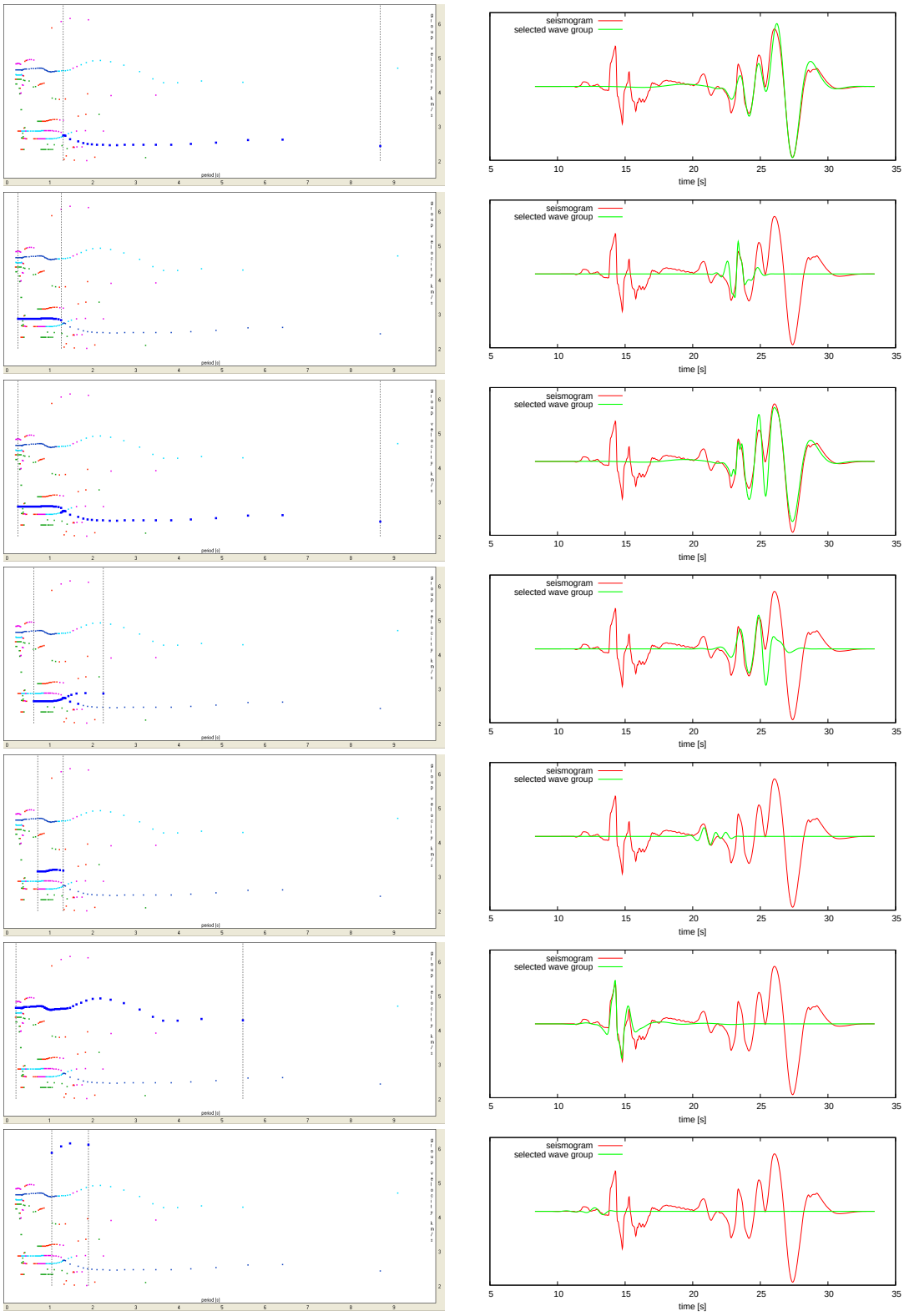

Figure 2.3: Demonstration of different selection of dispersion curve. In each row, the left panel comes from the SVAL program (the spectrogram panel, labeled "C" in Fig. 2.2), color points represent dispersion curves, the dark blue bold points are selected. Right panel shows the wave group corresponding to the selected dispersion curve (green). The analyzed record are synthetic data for station PDO calculated in model Novotny-LA3.

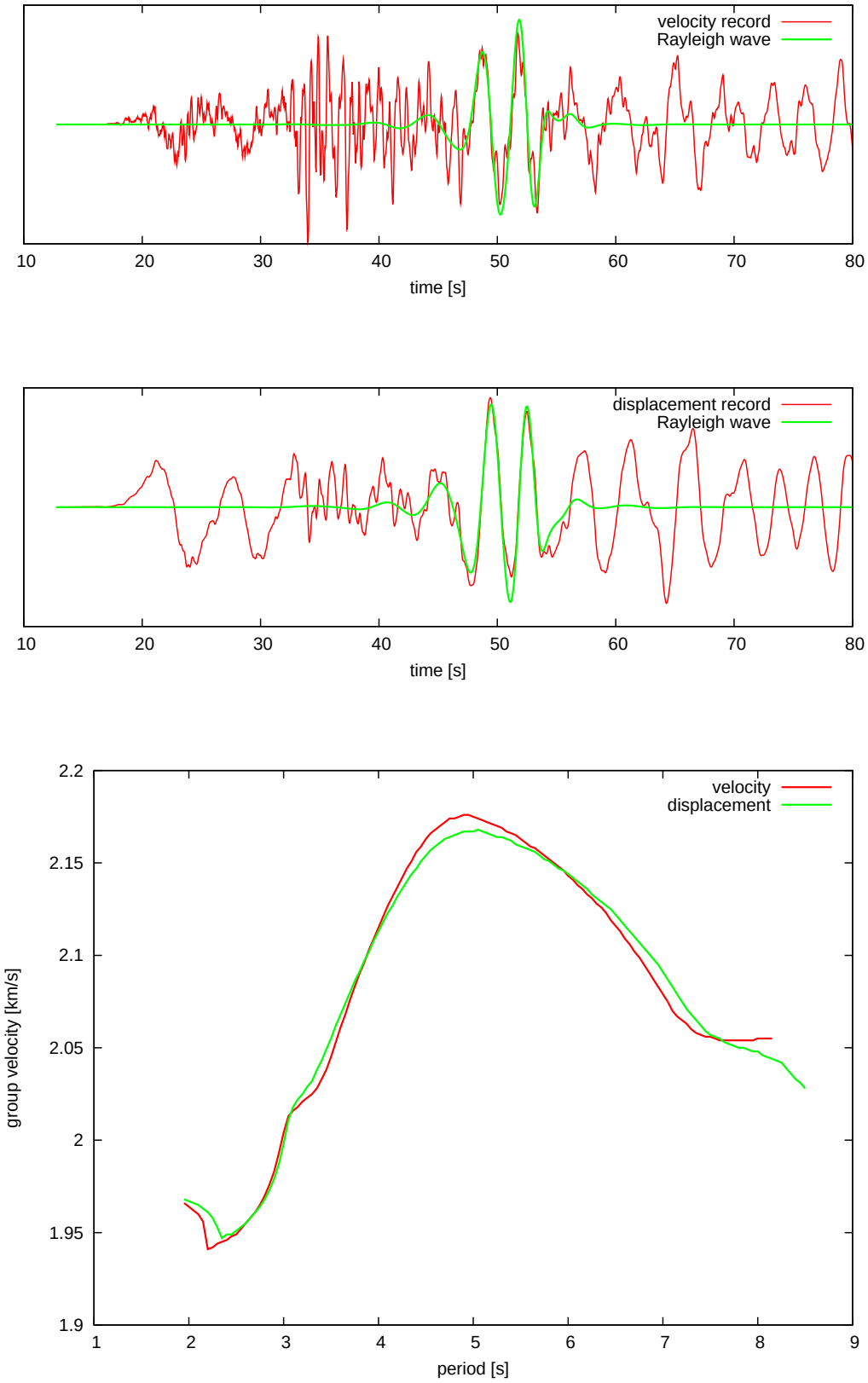

Figure 2.4: Top: Velocity record (real data at station LTK) analyzed by SVAL software with Rayleigh wave selected (green). Middle: Displacement record obtained by integration of the previous one analyzed in the same way. Bottom: Comparison of dispersion curves for the waves identified and highlighted (green) above. All parameters of the analysis of the velocity and displacement records were the same.

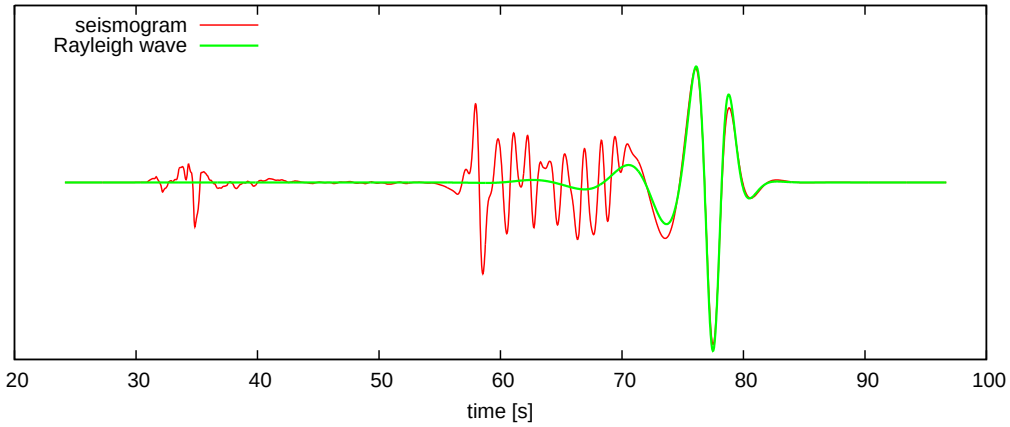

Figure 2.5: Synthetic test. Vertical component of synthetic "data" (red) and the wave group corresponding to the dispersion curve of the fundamental mode of Rayleigh wave determined by SVAL program (green). The "data" were generated by the DW method in crustal model Novotny-LA3 for station LIT (Litokhoron, epicentral distance 193 km). The 'experimental' dispersion curve is plotted in Figs 2.7–2.9. It is one of the cases well-fitting the theoretical dispersion curve.

Rayleigh wave fundamental mode (Fig. 2.5). We found that the identification of the 'ridge' may be sometimes problematic. It is especially the case of near stations where the fundamental mode might partially overlap with some higher modes. As an example, we compare the favorable and unfavorable situations in Fig. 2.5 (fundamental mode only) and Fig. 2.6 (overlapped modes), respectively. Corresponding dispersion curves are shown in Fig. 2.7.

Hereafter, we will use the word 'experimental' in quotation marks to refer to something obtained by dispersion analysis of synthetic seismograms, usually the dispersion curve.

The obtained 'experimental' dispersion curves for all stations were compared with the theoretical dispersion curve (independent of the station), calculated by program VDISP. As shown in Fig. 2.8, the largest difference between the 'experimental' and expected curves was at stations in epicentral distance less than 100 km.

The curves for more distant stations were much closer to each other, and also closer to the theoretical curve, but only in the period range 2–6 seconds, where the predominating periods of the Rayleigh wave are. For periods shorter than 2 s, and longer than 6 s, the curves differ as shown in Fig. 2.9. We hypothesize that it might be caused by week amplitudes of the wave at short and long periods. The theoretical dispersion curve does not include any information about amplitude. When a wave is extremely weak at some period, the theoretical curve still exists, but it is no chance to find the wave by numerical method (e.g. in SVAL), because it is negligible compared to the other modes and/or a noise (in the real records). This is an important warning that the dispersion curves coming from the frequency-time analysis may not always be simply related to the assumed wave mode (here shown for the fundamental Rayleigh mode), so should be used with a great caution.

Finally, we checked the agreement between dispersion curves obtained from

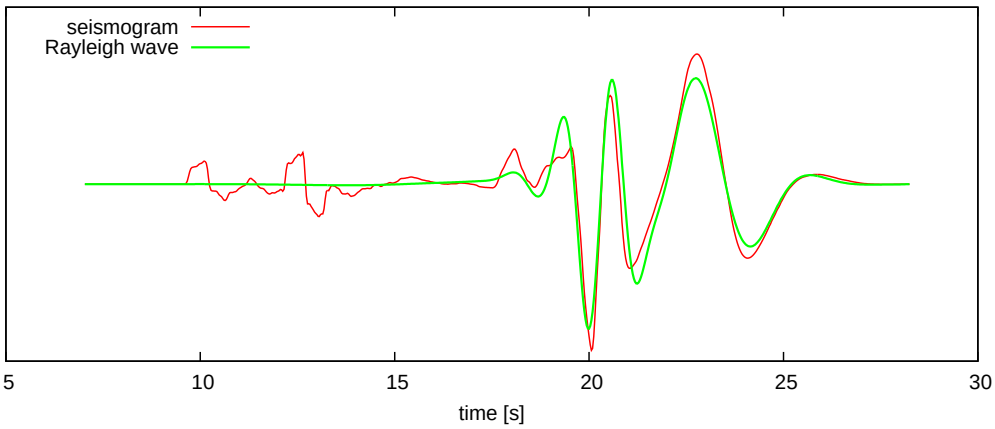

Figure 2.6: Similar synthetic test as in Fig. 2.5, but for station RLS (Riolos of Patras, epicentral distance 56 km). The identified wave (green curve) probably corresponds not only to fundamental mode of Rayleigh wave, but also to some higher modes. The 'experimental' dispersion curve is plotted in Fig. 2.7 and Fig. 2.8. It is one of the cases of poorly fitting with the theoretical dispersion curve.

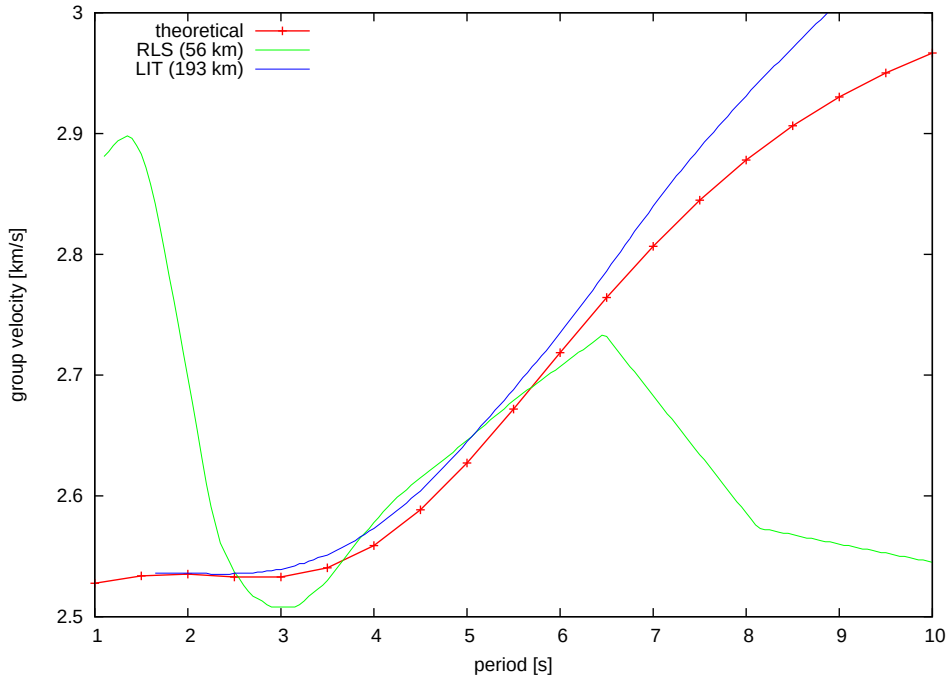

Figure 2.7: Synthetic test. Dispersion curves for records shown in previous Figs 2.5 and 2.6. The theoretical curve is shown for comparison. The favorable and unfavorable cases are illustrated for stations LIT and RLS, respectively.

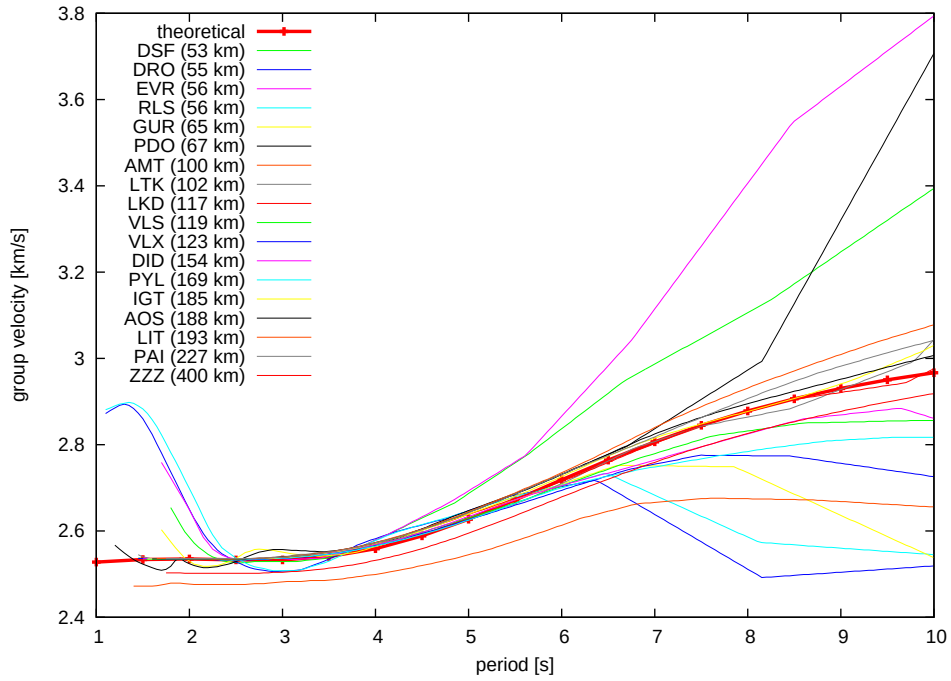

Figure 2.8: Synthetic test. The analyzed seismograms are synthetics calculated by the DW method. Vertical components are analyzed in SVAL as if they were real data. The curves from SVAL are compared with the theoretical dispersion curve calculated by VDISP (bold red). The curves for different stations should be theoretically identical, but the agreement is enormous. Most problematic are the stations with small epicentral distance. It can be explained by overlapping of the fundamental and higher modes of the Rayleigh wave.

the radial and vertical component. Interestingly, at a station, the 'experimental' curves for both components are nearly identical just in the period interval where they agree with the theoretical curve (see Fig. 2.10). It seems that the agreement between components serves as an indicator of the reliability of the 'experimental' dispersion curve.

2.5 Remarks to technical issues

Before plotting seismograms with selected wave groups like Figs 2.3–2.6 we had to normalize the amplitudes. The information about the amplitude of the selected wave group is not available from the SVAL program because overlapped Gaussian filters are used. We calculated the amplitudes of the selected wave group as to fit the analyzed seismogram by minimization of the difference in the L^2-norm.

We also need to plot arrows labeling approximate P- and S-wave arrival for basic orientation in the seismograms (e.g. as in Fig. 3.1). We calculated them by program HYPO (Lee WHK , 1989) in crustal model *Rigo* (described later in section 4.1).

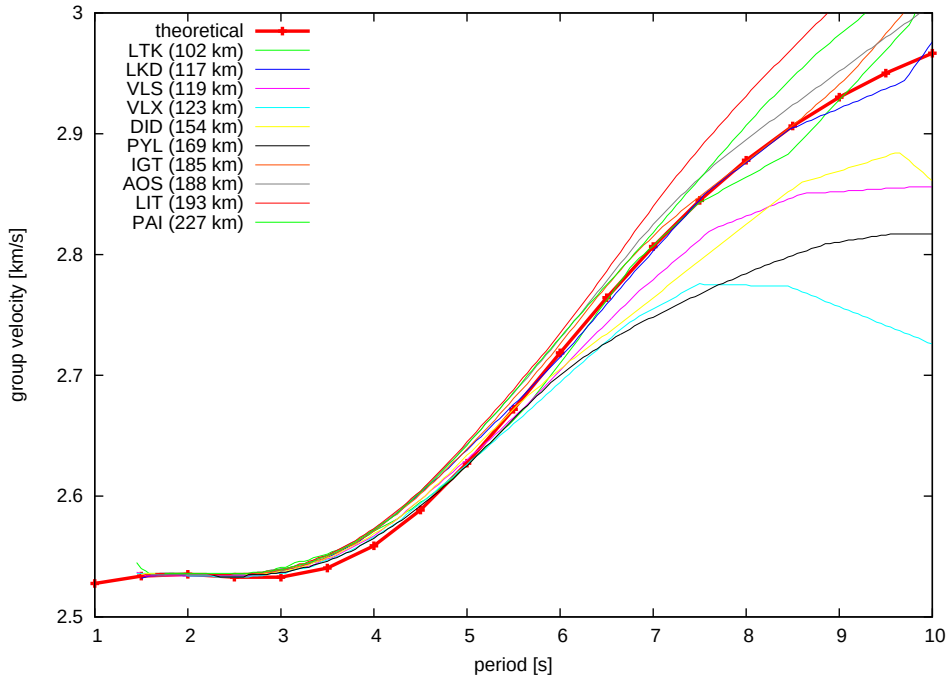

Figure 2.9: Similar comparison as in Fig. 2.8, but only for stations with epicentral distance greater than 100 km. Note a relatively good agreement between curves for different stations (solid lines) and the theoretical curve (solid line with points), but only in the period range 2–6 seconds.

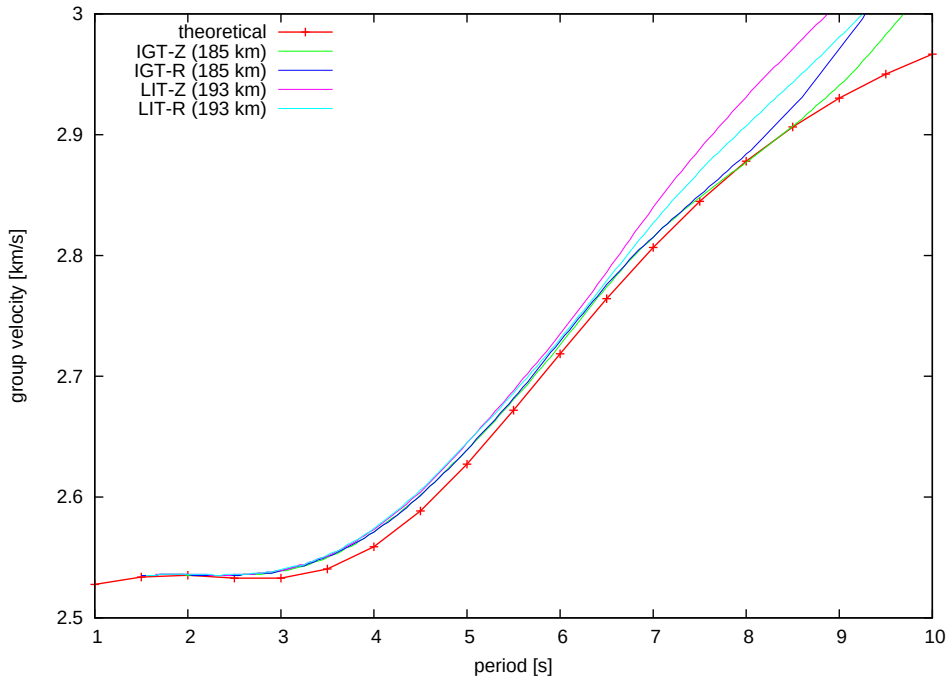

Figure 2.10: Comparison of the 'experimental' dispersion curves, calculated by program SVAL for radial and vertical components of the synthetic seismograms at two stations. The agreement between components is very good in the interval where there is also good agreement between the obtained curve and theoretical one.

3. Dispersion analysis of real data

In this chapter we apply the previously described programs to real data. We use experience acquired on analyzing synthetic data.

In the first step, the radial component of the velocity records from 21 seismic stations was analyzed by the SVAL program. The aim was to find dispersion curves for the FLP-waves. Then the obtained curves were compared to each other. The agreement between them was quite poor. At the end of this chapter, we discuss the possibility of finding any general characterization of the FLP-wave in terms of the experimental dispersion curve.

3.1 FLP-wave selection in spectrogram

The selection of a dispersion curve related with FLP-wave was done in spectrogram of program SVAL (panel "C" in the previous Fig. 2.2). Technically, we had to select all points of dispersion curve by mouse. A guess which points should be selected was required. We have always plotted wave group corresponding to the selected dispersion curve and noted down quality of result determined by eye (later quantified, see below). At some stations, we tried to select more variants of the dispersion curve.

The chance to find dispersion curve corresponding to the FLP-wave was strongly correlated with the FLP-wave amplitude. As a rule, there were no problems with stations featuring intensive FLP-wave (Fig. 3.1). Stations where the wave was weak were more problematic (Fig. 3.2), and, naturally, there was no chance to track the FLP-wave by frequency-time analysis in records, where we were not able to find it visually (Fig. 3.3). The map of the ability to construct the dispersion curve would look nearly identically as the map of the FLP-wave occurrence (Fig. 1.6).

We also wanted to quantify the reliability of results. It means to quantify if the FLP-wave was selected properly in the record. Correlation coefficient between the record and the selected wave group was used. A restriction was needed to avoid correlating strong surface waves with zero-line after end of the FLP-wave. We use the interval between P- and S-wave arrival as a proxy of the part of the record where the FLP-wave should be present.

The obtained correlation coefficients (Table 3.1) were compared to the fit quality determined by eye. In the most of cases it agrees. The coefficient would be probably useful (optionally in combination with some other criterion) if there will be a need to process a large amount of data.

3.2 Experimental dispersion curve of FLP-waves

As the first step, we compared all obtained dispersion curves (Fig. 3.4). The variation was very large; it resembled nearly randomly strewn points.

station	variant	correlation
MAM	R	72 %
MAM	Z	74 %
DSF	R	7 %
DRO	R	72 %
DRO	Z	54 %
EVR	R	76 %
RLS	R	85 %
GUR	R-1	51 %
GUR	R-2	52 %
AMT	R-1	35 %
AMT	R-2	57 %
AMT	Z	73 %
LTK	R-1	76 %
LTK	R-2	74 %
LTK	Z	56 %

station	variant	correlation
LKD	R	40 %
VLS	R	20 %
VLX	R	83 %
VLX	Z	68 %
DID	R	49 %
PYL	R	82 %
PYL	Z	69 %
IGT	R	52 %
AOS	R-1	60 %
AOS	R-2	31 %
LIT	R-1	67 %
LIT	R-2	49 %
PAI	R-1	70 %
PAI	R-2	43 %

Table 3.1: Correlation coefficient between the record and the wave group corresponding to the dispersion curve of the FLP-wave. Letter 'R' in the column 'variant' means the radial component, letter 'Z' means vertical component and symbols '1' and '2' mean that the radial component was analyzed twice.

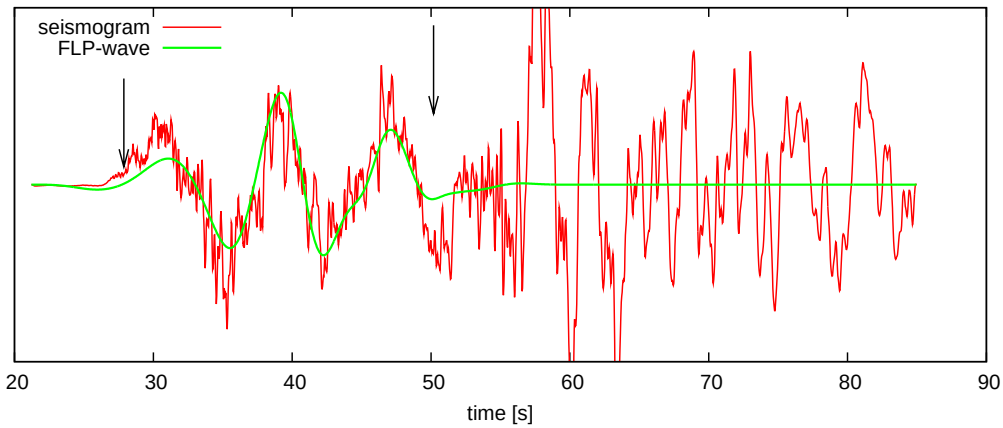

Figure 3.1: Radial component of observed seismogram (red) for the Efpalio earthquake at station PYL (Pylos, epicentral distance 170 km). The wave group corresponding to selected dispersion curve (green). Black arrows mark the arrival times of P-wave and S-wave calculated in model Rigo (Rigo *et al.*, 1996) for hypocenter location from Table 1.1. The dispersion curve is a part of Fig. 3.6

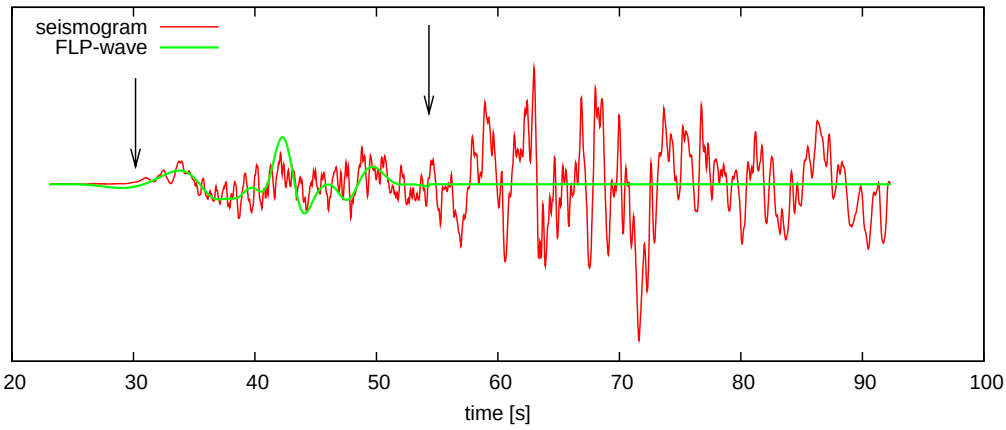

Figure 3.2: Similar example as in Fig. 3.1. Radial velocity record (red) at station IGT (Igoumenitsa, epicentral distance 185 km) and the wave group corresponding to selected dispersion curve (green). The question whether we have selected the FLP-wave or not is open.

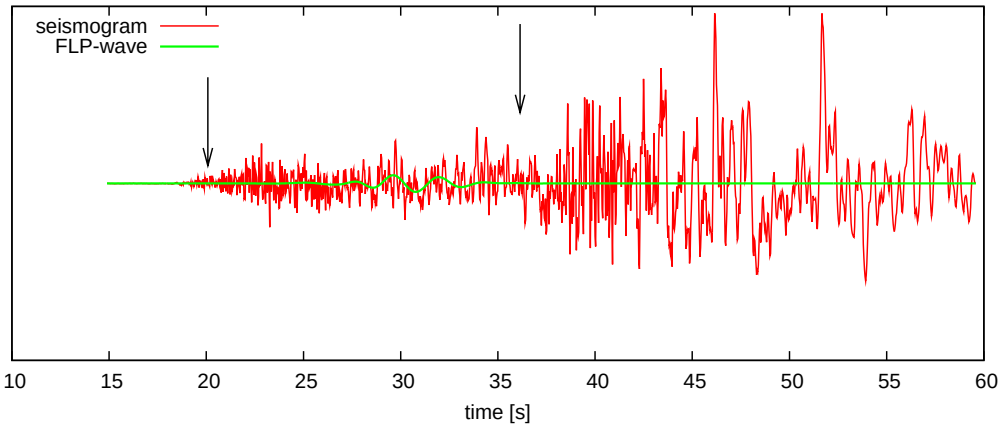

Figure 3.3: One of unsuccessful cases. Radial velocity record (red) at station VLS (Valsamata, epicentral distance 119 km) and the wave group corresponding to selected dispersion curve (green). There are not many reasons to believe that highlighted wave group is the FLP-wave.

To obtain a better insight into the variation, we removed the most problematic stations, i.e. those at which we have noted that the result is not reliable while selecting the dispersion curve. In the remaining curves we made a further selection; in case that two variants of the dispersion curve was available at a stations, we have chosen that one whose corresponding wave group better meet our idea of "ideal FLP-wave". It usually meant that one with higher correlation coefficient. Looking back at corresponding wave groups of dispersion curves at Fig. 3.4, the explanation of extremely high difference between curves might be found. Probably, there were points corresponding to dispersion curves of different waves mixed together.

With this selection, a significantly simpler pattern of the dispersion curves was obtained (Fig. 3.5), allowing identification of 3 strips. To check whether the three strips are reliable, we further selected only four curves from the stations with the strongest FLP-waves, where we were sure that the identification of the dispersion curve (by selecting its 'ridge' in the spectrogram) had been made properly (Fig. 3.6). The agreement between two of them (DID and VLX) is very good, but the other two curves (LTK and PYL) differ significantly. DID, VLX and the short-period part of PYL belong to the upper two strips of Fig. 3.5, while LTK and low-period part of PYL belong to the lower strip.

We made also another test. For all 4 stations of Fig. 3.6 we compared the dispersion curves for the vertical and radial components. The agreement between the components was much better that between the different stations. Fig. 3.7 demonstrates such a test for station LTK. It indicates that the dispersion curves of Fig. 3.6 are reliable, so probably also the strips in Fig. 3.5.

3.3 Result of dispersion analysis

We believe that the key to understand the experimental dispersion curves of the FLP-way is in Fig. 3.5. If we focus on the period range between 4–8 seconds, typical for the predominant period of the FLP-waves, we can see that the experimental points split into 2 to 3 strips. The slow strip seems to be dominated by the stations at epicentral distances smaller than 110 km. (Epicentral distance of the station AOS, also belonging to the slow strip, is 188 km, but the FLP-wave is weak at the AOS dispersion curve is not reliable.) The fast strip of dispersion curves is dominated by the more distant stations. The recognition of the split of the dispersion curve into strips is the most important result of the empirical part of this thesis.

Although the epicentral distance might determine the strips, effects of the lateral crustal heterogeneity represent an important alternative explanation.

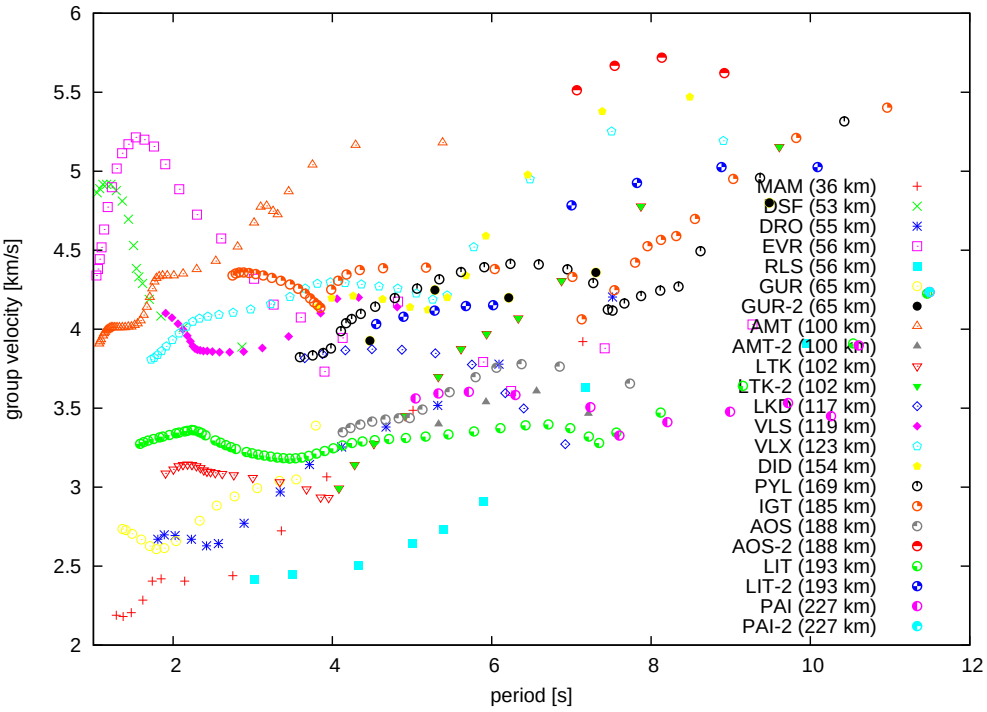

Figure 3.4: Results of dispersion analysis of fast long-period wave in real seismograms for radial component at 17 stations. Some of them were investigated twice with different dispersion curves selected (e.g. 'GUR' and 'GUR-2').

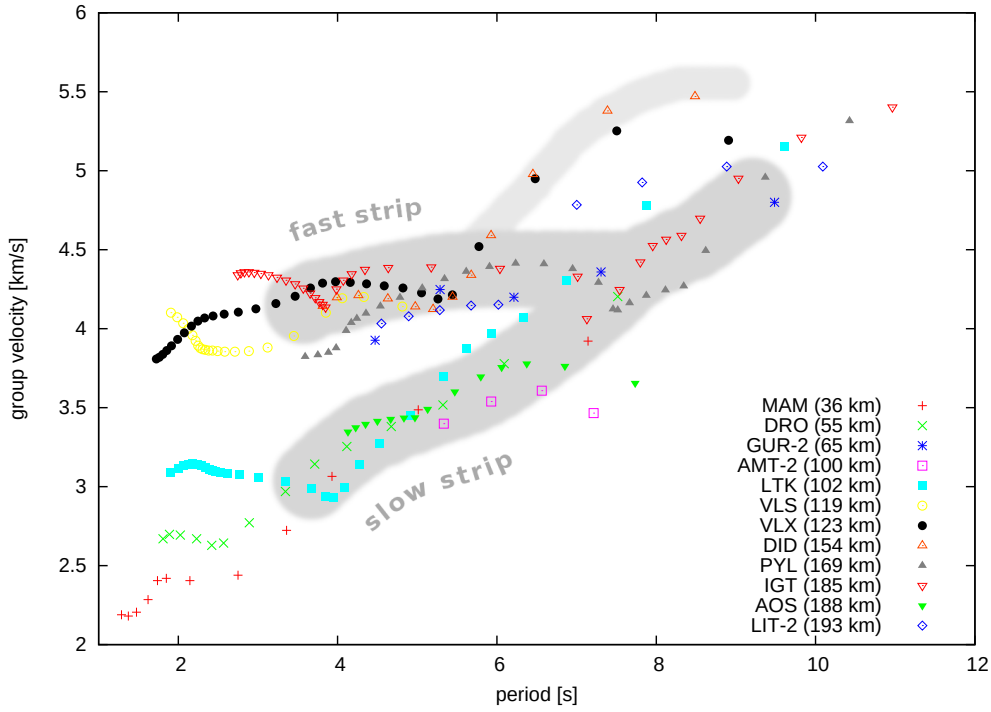

Figure 3.5: The same plot as in Fig. 3.4, but most problematic curves (in terms of correlation coefficient and quality of the FLP-wave selection determined by eye) were excluded, and for each station only one variant of the curve was used. We hypothesize that dispersion curves split in three strips (gray). Two major strips join at periods longer than 7 seconds.

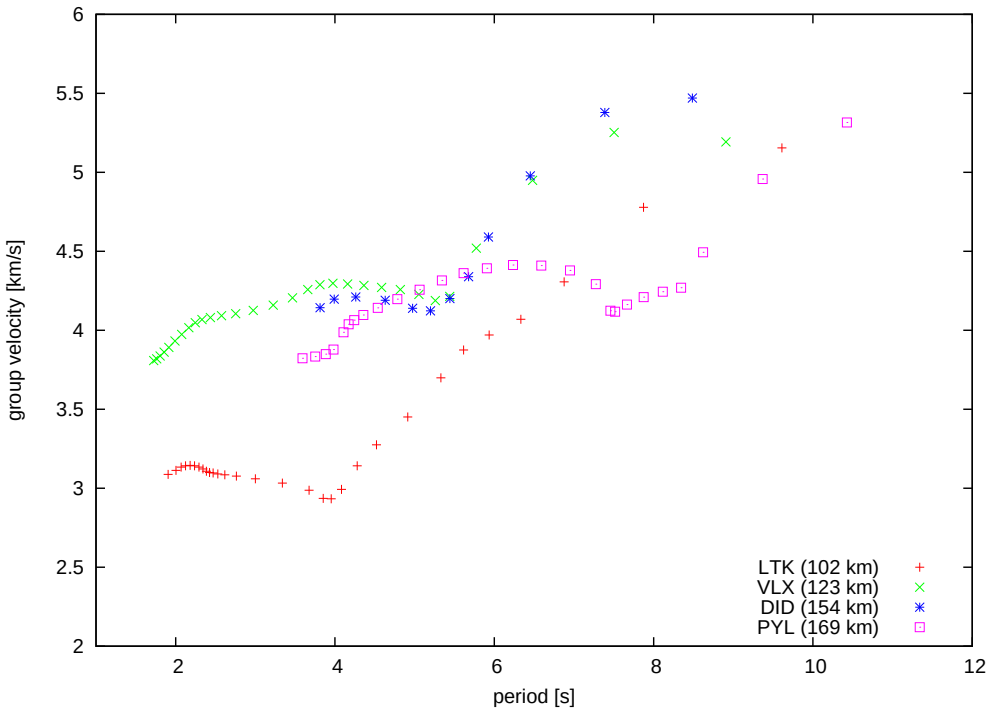

Figure 3.6: The same plot as in Figs 3.4 and 3.5, but only dispersion curves for 4 stations, which we believe to be the most reliable. The agreement between dispersion curves for stations VLX (epicentral distance 123 km, azimuth 161°) and DID (epicentral distance 154 km, azimuth 131°) is very good.

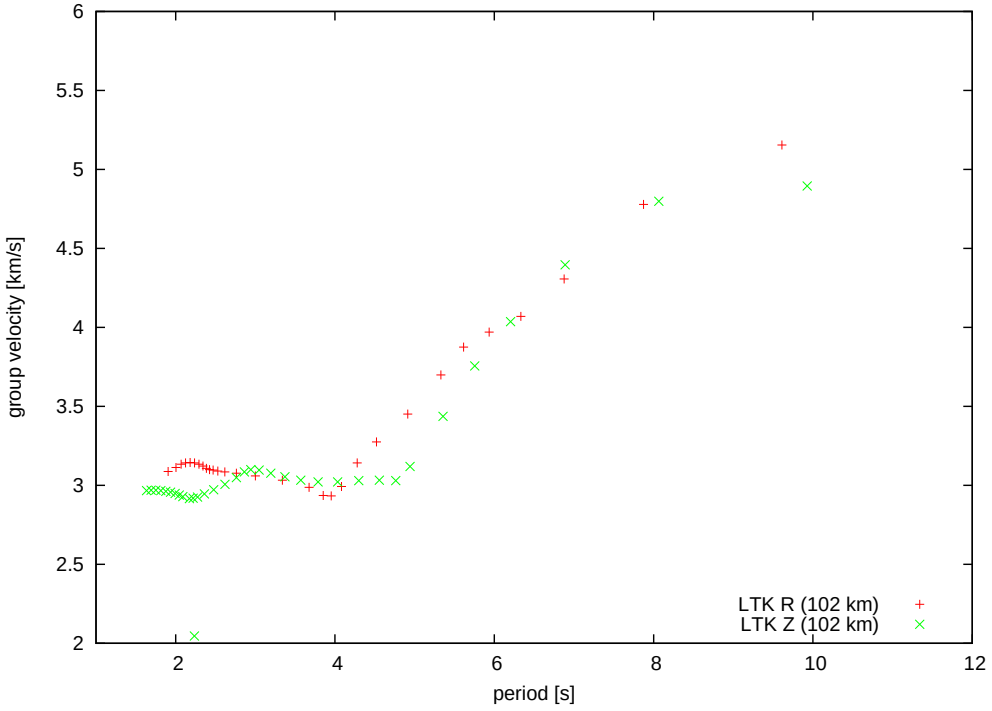

Figure 3.7: Comparison of the dispersion curves obtained by the analysis of radial and vertical component of record at station LTK. The agreement between the two components is very good (much better than between curves obtained at different stations). It indicates that these dispersion curves are determined well.

4. Sensitivity study

The aim of this chapter is to make a first guess of the crustal model, in which the FLP-waves are likely to be generated. This is a prerequisite for the structural inversion made in the next chapter.

We started with generating synthetic seismograms in existing crustal models. We also tried to create models with some special properties which, according to our feeling, could generate the FLP-wave. After testing dozens of models, mostly producing seismograms with a very weak FLP wave, if any, we selected a class of a few models which generated records similar to real data. Then we tried to find common features of these models, to define likely parameters which mostly influence the occurrence and strength of the FLP-wave. The result is a set of parameters of the crustal model at which FLP-wave is sensitive.

4.1 Synthetic seismograms for existing models

We proceeded from existing crustal models (Fig. 4.1) of the studied region.

The forward modeling of synthetic seismograms was performed by the DW method, using a special interface developed for this work. The interface, described in section 2.1, makes calculation and plotting easy, and the results are automatically arranged in hierarchical directory structure. The synthetics were calculated for frequencies up to 10 Hz.

The FLP-waves occurrence in the models mentioned above was not satisfactory, so we evaluate the waves only qualitatively. Roughly in one half of the models the FLP-waves were weak compared to the real data (Fig. 4.2). In some models the FLP waves were not present at all (Fig. 4.4, bottom part). We tried some other experiments, such as changing v_P/v_S ratio in different layers or adding a low-velocity layer at the top of the existing models. We also checked a shallower source depth. None of these experiments succeeded noticeably better.

Then, more or less by chance, in relation to another study, we tried a model reported for east Turkey. It is the so-called CLDR model (see Fig. 4.3), obtained by joint inversion of receiver function and dispersion curves of surface waves (Gök *et al.*, 2011, G. Ameri, personal communication). Not only the FLP-wave occurred in the synthetic seismograms, but also the agreement between the initial part of the synthetic and observed seismogram (between the P- and S-wave onset) was good. The CLDR model has several characteristic features – the low velocity channel in the middle crust and the low velocity layer at the top are the most distinct ones.

We wanted to prove or disprove the idea, that the FLP-wave is controlled by the low velocity channel. We altered the model removing the channel, thus making v_P a non-decreasing function of depth. As v_P/v_S ratio is constant in the model, it implies that v_S is non-decreasing, too. The FLP-wave remained nearly unchanged (Fig. 4.4, middle part). The following test proved an idea, that the key parameter for this wave is low velocity layer at the top of the crustal model and velocity contrast on bottom boundary of the layer.

We made up more models with similar behavior (in the sense of the FLP-wave properties), all of them had one or more low velocity layers within 4 km bellow

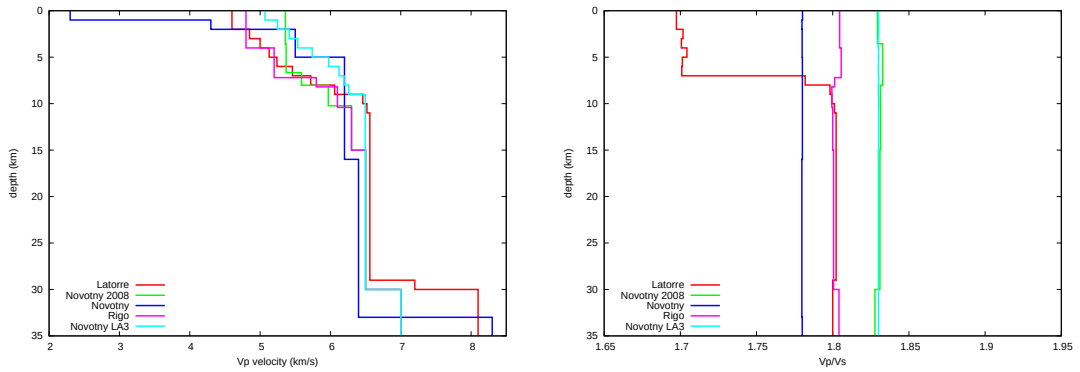

Figure 4.1: Crustal models for the studied region used to compute synthetic seismograms. Novotny (Novotný *et al.*, 2001), Novotny 2008 (Novotný *et al.*, 2008), Rigo (Rigo *et al.*, 1996), Latorre (Latorre *et al.*, 2004) and Novotny LA3 (Novotný *et al.*, 2012). The latter model is most relevant for this study because it was obtained from simultaneous inversion of the structure and location, based on P and S arrival times of the Efpalio 2010 earthquake sequence.

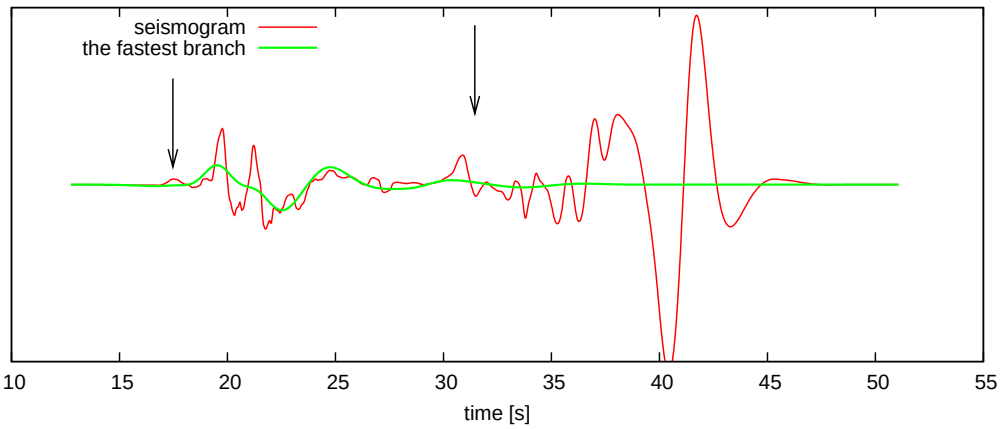

Figure 4.2: Simulated "data" (red) and the extracted wave group (green). The extracted wave group corresponds to the fastest dispersion curve of the "data". "Data" were generated for a point source with parameters similar to the Efpalio earthquake: the triangular time function, duration 1 second, depth 6.6 km, other parameter according Table 1.1. Crustal model Novotny-LA3 was used. Black arrows mark the arrival times of the first-arriving P- and S-wave calculated in model Rigo.

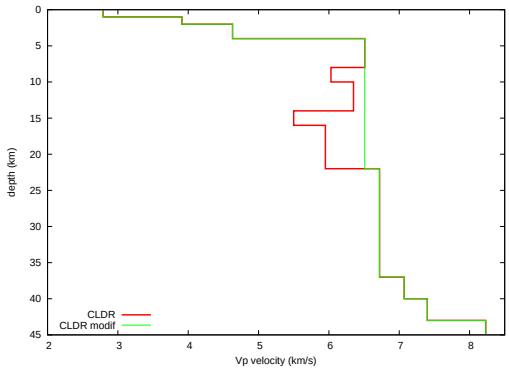

Figure 4.3: Crustal model CLDR (red) and its modified version with the low velocity channel removed (green).

the Earth surface and distinct step in v_P velocity under it. The CLDR model (both original variant and version with low velocity channel removed) belongs to the set of suitable models.

4.2 Results of sensitivity analysis

After many tests of different parameters, which might affect the FLP-wave occurrence and strength, we believe that the wave is controlled by relatively shallow part at the top of the crust (depth less than 5 km). The velocity contrast on the bottom boundary of such a 'layer' is also important.

The agreement between real and synthetic seismograms is not very good (Fig. 4.5), we do not want to say that we have found a model where the FLP-wave can be generated as strong and with the same characteristic as in the real case. The goal of this part of study is a set of parameters which control the FLP-wave properties. It is also the reason why we do not quantify the FLP-wave "quality" or amplitude in different models – there is no need to say which model is the best, if none of them is good. Definitely more important is the fact that all suitable models have the same feature.

The next step will be inversion of the uppermost part of the crust and discussion about influence of the v_P/v_S ratio, which we kept fixed constant in the whole crustal model yet.

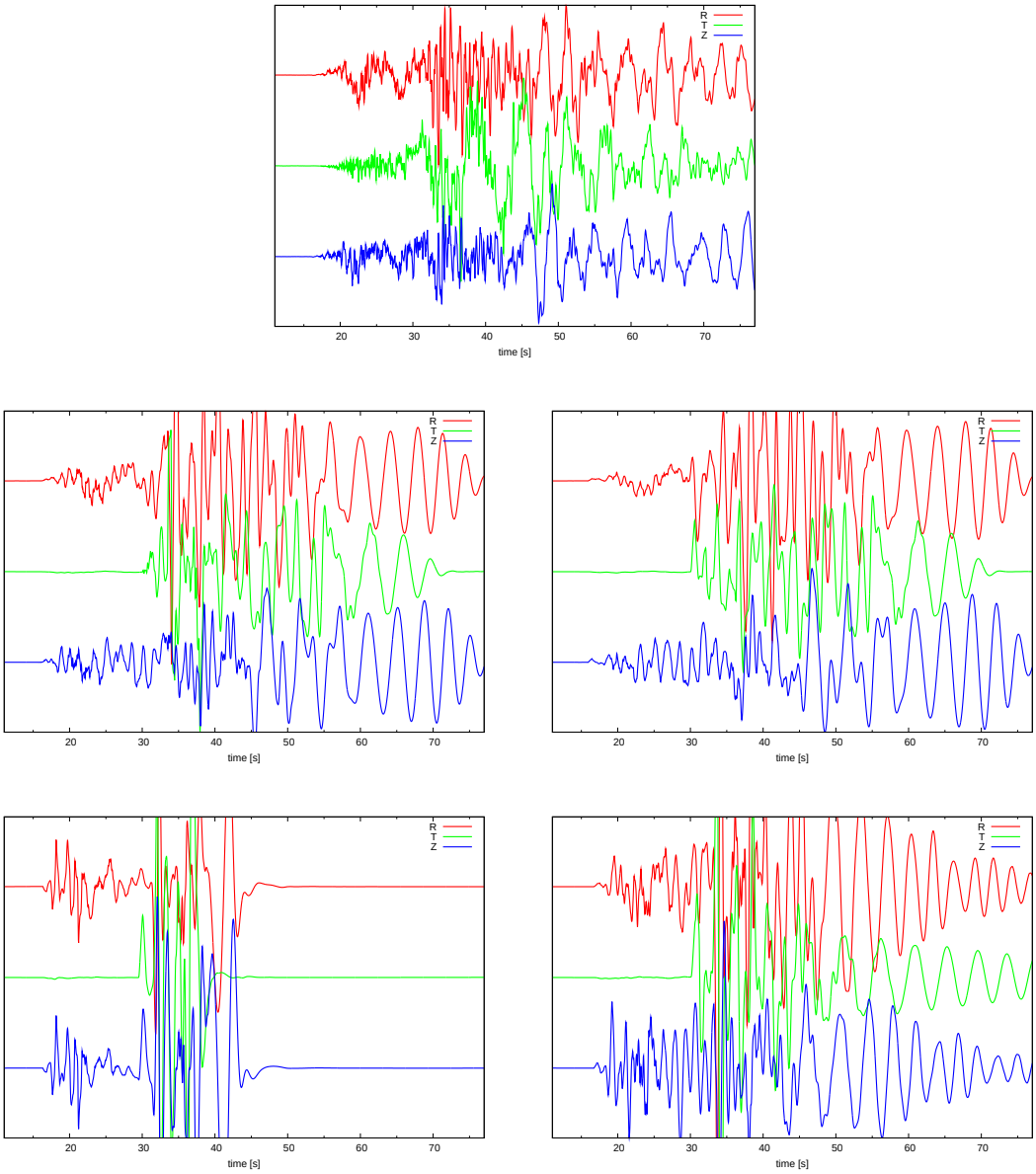

Figure 4.4: Real velocity record (top) compared to synthetics in different models; station LTK, epicentral distance 102 km, frequency range of the synthetics 0.02–10 Hz: CLDR (middle left) and its modified version with the low velocity channel removed (middle right), Latorre (bottom left) and Novotny (bottom right). The FLP-wave is notable in both variants of the CLDR model; its amplitudes related to the real case of the FLP-wave are about 70 % and 50 %, respectively. The predominant periods of the observed and calculated FLP-waves are nearly the same. The synthetics were computed for parameters similar to the real case of the Efpalio earthquake (according Table 1.1 and triangular time function, duration 1 second). The amplitude scale remains the same in all seismograms.

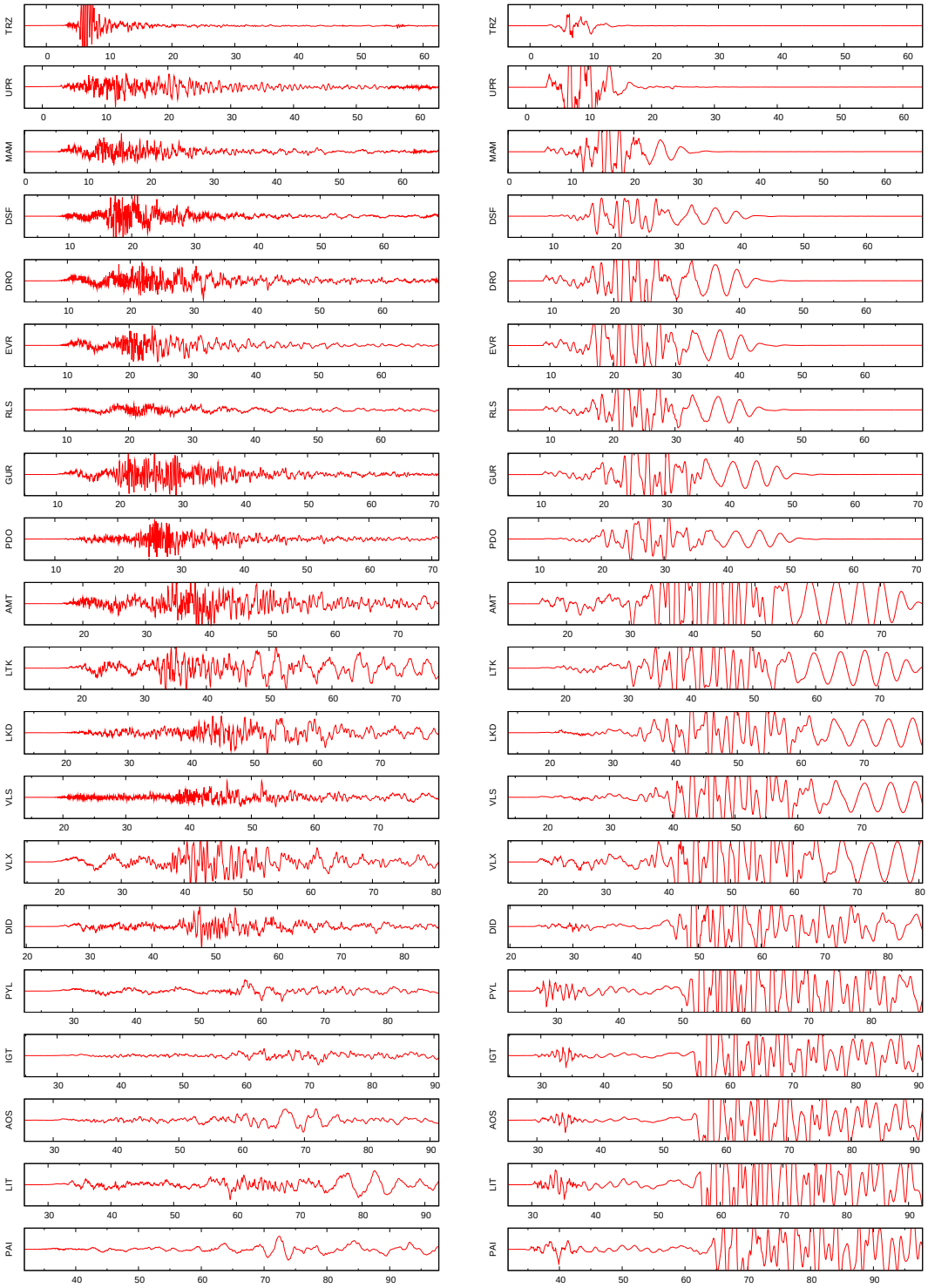

Figure 4.5: Radial component of real velocity records at all 21 stations (left) compared to synthetic seismograms (right) calculated in the CLDR model (version with the low velocity channel removed). The FLP-wave in real and synthetic records are present at some of stations, especially at DRO, EVR, AMT, LTK, ..., but not at all of them, indicating possible effects of the radiation pattern. The stations are sorted by their epicentral distance. The amplitude scale differs from station to station, but remains the same at corresponding synthetic and real record. Note that the seismograms have been approximately aligned with respect to the first arrivals.

5. Inversion of the shallow crustal structure

One of the aims of this thesis is to create a crustal model explaining the observation – both the dispersion curves and seismograms. In this chapter, we perform inversion of the uppermost part of the crust. Concentrating on the shallow part has two reasons: it was indicated by the sensitivity analysis, and it increases stability of the inversion compared to the whole-crust inversion.

In the first section the Neighborhood algorithm is described. We chose this method because of its ability to solve global optimization problem of a function with many local minima; moreover, it is an easily applicable code, verified elsewhere. In the second section we formulate the inverse problem and define its parametrization. The results are shown and discussed in the third section. Finally, we derive the dispersion curve from synthetic records in the best fitting models, following exactly the same procedure as with real data, and we compare the synthetic dispersion curve with the experimental ones, obtained in Chapter 3.

It is to mention that there are two different approaches how to find crustal model explaining some waves (the FLP-wave in our case). The first possibility is an inversion based on searching for model with best similarity between observed and theoretical dispersion curve of the selected mode or modes. The second approach is inversion based on agreement between the real seismograms and synthetics in tested model. When starting work on this thesis, we planned to perform inversion of the experimental dispersion curves. However, when recognizing problems with their determination we decided to invert directly the seismograms. Comparison of the dispersion curves, that we perform at the end, thus represents an independent validation of the obtained crustal models.

5.1 Neighborhood algorithm

The Neighborhood algorithm, introduced by Sambridge (1999), is a derivative-free search method for finding model of acceptable data fit in a multidimensional parameter space. It belongs to group of a global optimization methods, such as simulated annealing and genetic algorithms. The goal of NA is to find an ensemble of models that preferentially sample the good data-fitting regions of parameter space, rather that finding a single best-fitting model.

The idea of algorithm is to solve the forward problem in randomly selected n_s points (samples) in data space and construct 'approximate misfit surface'. Then to select next n_s points in regions with lower misfit, solve the forward problem in them and improve estimation of misfit surface using all n_p points where the forward problem have been solved so far. The density of sampling increases in regions of lower misfit in every step, so we are approaching the minimum.

The 'approximate misfit surface' is realized by geometrical construct known as Voronoi diagram. This is a unique way of dividing multidimensional space into n_p cells (convex polyhedrons). Each cell is simply the nearest neighborhood region of a sample. The L^2 norm is used to measure distances. The approximation of misfit surface is generated simply setting the misfit constant in each cell.

Selecting next n_s points is done by selecting n_r cells of lower misfit and performing a uniform random walk in each cell (generating n_s/n_r new points in the cell).

The advantage of using this algorithm is that we have only three tuning parameters n_s, n_r and number of iterations. The algorithm has ability to select intelligent and effective way of sampling model space itself.

This algorithm does not require any scaling of misfit function, any combination of data fit criteria can be used. The misfit value is only compared between different models, its absolute value is not important.

5.2 Inverse problem formulation

We use the DW method as the forward solver, so we are limited to layered models only.

First of all, we need to prescribe values for those parameters which we do not want to determine by solving inverse problem. They include the density and quality factors in the studied shallow part, as well as all parameters of the deeper part (below the of 4-km depth). As for the deeper part we used the so called 'average model', see Tab. 5.1 (Vladimír Plicka, personal communication). It was obtained by the Neighborhood algorithm from waveform inversion of the Efpalio earthquake, using records at 8 near-regional stations and frequencies between 0.05–0.2 Hz.

depth [km]	v_P [km/s]	v_S [km/s]	ρ [g/cm^3]	Q_P	Q_S
0.0	5.12	2.75	2.7	300	150
1.2	5.25	2.82	2.7	300	150
3.0	5.31	2.85	2.9	300	150
4.0	6.07	3.27	2.9	300	150
4.2	6.39	3.43	3.0	300	150
12.0	6.40	3.44	3.0	300	150
27.1	6.88	3.70	3.1	300	150

Table 5.1: The 'average model' obtained from full waveform inversion of the Efpalio earthquake observed at 8 stations (Vladimír Plicka, personal communication). The inversion performed in this thesis keeps unchanged the model in its lower part (below the double line).

We introduce 2 parametrizations (see Table 5.2). The first one (hereafter referred as parametrization A) uses 3 layers of nearly arbitrary depth in uppermost 4 km of the crust. We invert for the layer thicknesses, v_P and v_P/v_S ratio in each layer. There is one constraint, so only 2 values of the thickness are required, hence the model has 8 parameters. There is an additional constraint on v_P velocities that prohibits the low velocity channel in v_P. But the v_P/v_S ratio may differs from layer to layer, so that the low velocity channel in v_S is possible.

The second parametrization (hereafter referred as parametrization B) has again 3 layers, total thickness 4 km, we invert for layers thickness, v_P velocities and v_S velocities. The number of free parameters is 8. In contrast to parametrization A both the v_P and v_S low-velocity channel is prohibited.

parametrization A — 8 parameters total

parameter		range	constraint
thickness	layer 1	0.1–2.0 km	total thickness 4 km
	layer 2	0.1–1.9 km	
	layer 3	arbitrary	
v_P	layer 1	2–5 km/s	no low-velocity channel
	layer 2–3	arbitrary	
v_P/v_S	layer 1–3	1.41–3	—

parametrization B — 8 parameters total

parameter		range	constraint
thickness	layer 1	0.1–2.0 km	total thickness 4 km
	layer 2	0.1–1.9 km	
	layer 3	arbitrary	
v_P	layer 1	2–5 km/s	no low-velocity channel
	layer 2–3	arbitrary	
v_P/v_S	layer 1	1.41–3	no low-velocity channel
v_S	layer 2–3	arbitrary	

Table 5.2: Parametrizations of inverse problem used. The only difference between parametrization 'A' and 'B' is v_S low-velocity channel enabling and disabling, respectively. The constraint on low-velocity channel also mean that the velocity in the third layer cannot be higher than the velocity down to 4 km in 'average model' (Table 5.1).

We use the DW method with interface developed by Jiří Zahradník for repeated forward modeling, which includes also adjustment of the origin time to optimize the waveform match. It was combined with the NA algorithm into a single inverse problem solver by Vladimír Plicka and the parametrizations were implemented by author.

The synthetic seismograms were compared to corresponding real records using an identical filter. We use acausal 4-parameter bandpass filter 0.02-0.05-0.20-0.30 Hz, which is flat between 0.05 and 0.20 Hz, while there are cosine tapers at the edges. The misfit function is the L^2-norm difference between the synthetic and real seismograms. The intention was to emphasize the initial part of seismogram between the approximate P- and S-wave arrival, where the FLP-wave occurs, so we upweighted the seismogram difference by factor 10 in that range.

Specifically, the misfit function is defined as

$$m = \frac{\sum_{stat} \sum_{comp} \int W(t, stat) \left(o(t) - s(t)\right)^2 dt}{\sum_{stat} \sum_{comp} \int W(t, stat) o(t)^2 dt} , \tag{5.1}$$

where m is the misfit function, t is time, $o(t)$ and $s(t)$ is observed and synthetic seismogram, respectively, $W(t, stat)$ is weighting function (used to emphasize the interval between P- and S-wave arrival) and *comp* stands for summing over seismogram components (N, E, Z or R, T, Z) and *stat* stations. The function gives zero value if the observed and synthetic seismograms are identical, higher

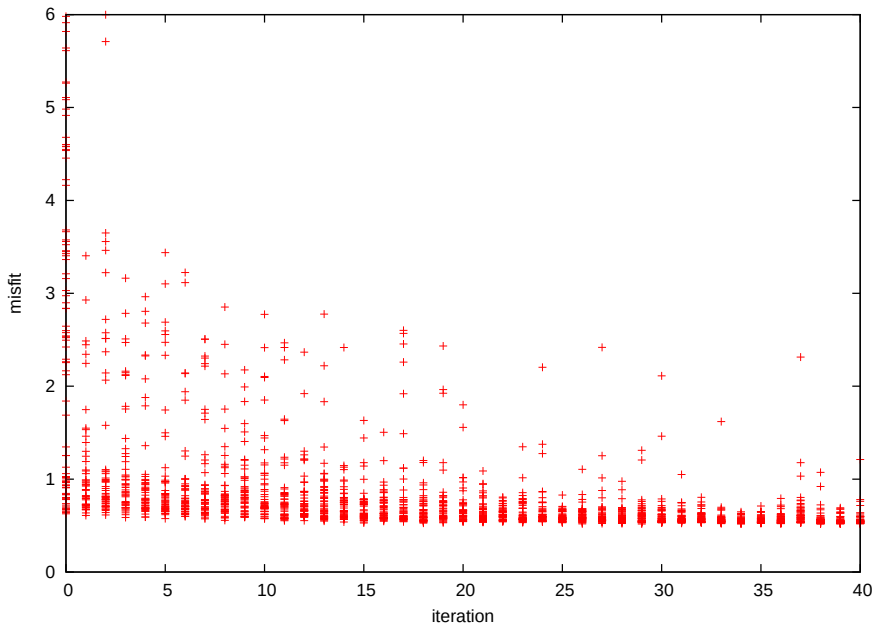

Figure 5.1: Development of the misfit value as a function of the number of iterations.

value mean worse agreement between the seismograms. If setting $W = 1$ for each time, the misfit function is equal to $[1 - \mathit{variance\,reduction}]$.

5.3 Results and their rating

In this section we will describe some results of the inversion, both for individual stations and for some groups of them. We would like to mention that we report the results in the order which should be logical for reader, although they were computed in slightly different order and some of them in parallel.

After a few tests, we used configuration of the NA method described in Table 5.3.

number of iterations	40
sample size for first iteration (n_{s0})	100
sample size for all other iterations (n_s)	50
number of cells to re-sample (n_r)	20

Table 5.3: Configuration of the NA algorithm used for inversion.

For the confirmation that the configuration was chosen properly, we checked dependence of misfit of samples on the number of iterations. Fig. 5.1 shows that the algorithm converged from sampling with a wide range of misfit values into sampling a region with an almost uniform and relatively small misfit.

First of all, we tried to perform inversion for single stations. We have chosen 4 stations with different epicentral distances and azimuths where the FLP-wave is well-developed, namely EVR (56 km, 351°), LTK (102 km, 115°), VLX (123 km, 161°) and PYL (170 km, 185°). We used parametrization 'A' (Table 5.2).

For each station, we plotted all models met by NA method, i.e. for which the forward problem was solved, and we classified them by color according the misfit value. That gives us an insight into models uncertainty. The results are shown in Fig. 5.2 and also in Fig. 5.3 with slightly different parameters (the difference described later).

The choosing proper color palette was quite a challenge. As it is evident from Fig. 5.1, most of models, where the misfit function was evaluated, lie very close to the optimal one. Moving to worse values, less and less models were calculated. Finally we found an optimal division of models into sets displayed by different colors. The best one includes models, whose misfit is not worse than 0.5 % of optimal misfit. Every next set size increases by powers of two, i.e. second set includes misfit not worse than 1 % of optimal one, the next 2 %, 4 %, 8 %, ... If we label optimal misfit value m, the interval of these sets are namely:

$$\begin{aligned}(m; 1.005m\rangle,\ (1.005m; 1.01m\rangle,\ (1.01m; 1.02m\rangle,\ (1.02m; 1.04m\rangle \ldots \\ \ldots (1.16m; 1.32m\rangle,\ (1.32m; \infty)\ .\end{aligned} \tag{5.2}$$

As it is apparent, e.g. from Fig. 5.4, the agreement between the FLP-wave in the real record and synthetic one (calculated in the best model found by the inversion) is very good, much better than in any models used for sensitivity testing.

Another significant observation is that the models for the four stations are very different, not only quantitatively, but also qualitatively (see Fig. 5.3). Model for station EVR has a very thin low-velocity layer bellow surface and high v_P/v_S ratio in the rest of inverted 4 km. Model for station LTK is characterized by a low-velocity channel for the S-waves between 3 and 4 km. Model at station VLX has nearly no v_S channel in the uppermost 4 km, but it results in drop of v_S at 4 km where the inverted zone is coupled with the fixed zone below. Both models for VLX and PYL have a relatively thick layer with low v_S velocity (leading to v_P/v_S about 3) in the middle part of inverted zone of the upper crust. The common feature for all stations is a layer with high v_P/v_S ratio, at most of stations (except station LTK) with thickness from 2 to 3.5 km and v_P/v_S between 2.5 and 3. This layer is overlain by a layer with lower v_P/v_S, leading to higher v_S than in the layer under it. We do not name it a low velocity channel; more accurate description is that a thin layer with high v_S lies below the surface. Comparing all four models, the most reasonable seems to be model at station PYL, featuring reliable boundary at bottom of inverted part of crust and not so high v_P velocity as the other models.

Models shown in Fig. 5.2 were calculated with a trial source delay varying between -1.8 and 1.8 seconds with respect to the origin time in Table 1.1. It means that the calculated synthetic seismogram can be shifted in both directions to find the best fit during each step of the NA testing. This might compensate uncertainty of origin time and source depth. But the found value was systematically at the upper limit of the enabled range. So we decided to disable shifting and perform the inversion again. Thus, we obtained Fig. 5.3. Compared to Fig. 5.2, we can see that all characteristic features remain the same, just the depths of the layer boundaries and velocities slightly changed and the misfit is higher.

The next question was whether there is a model, which can satisfactorily explain the FLP-waves at these 4 stations simultaneously. We performed their

Station EVR (epicentral distance 56 km, azimuth 351°), misfit 0.23

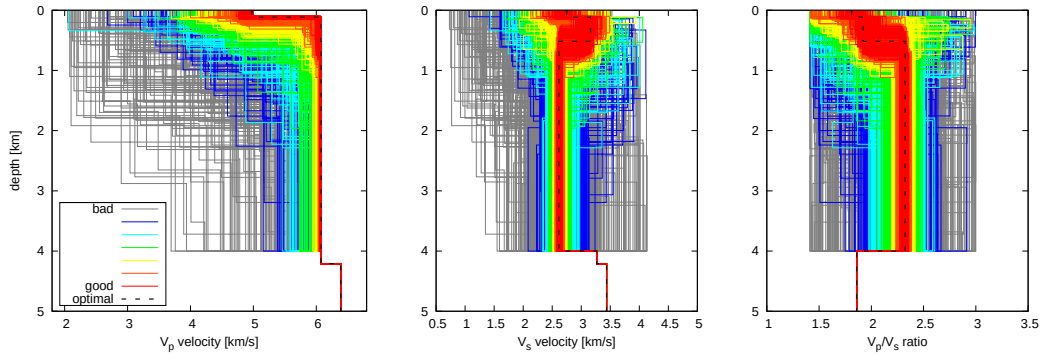

Station LTK (epicentral distance 102 km, azimuth 115°), misfit 0.52

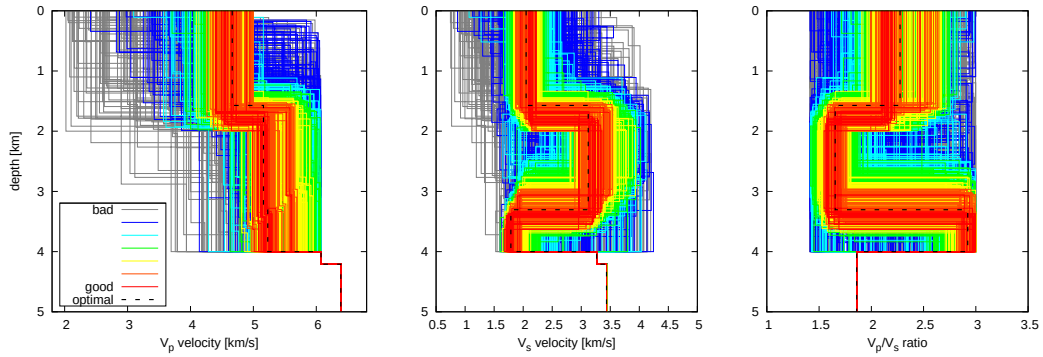

Station VLX (epicentral distance 123 km, azimuth 161°), misfit 0.46

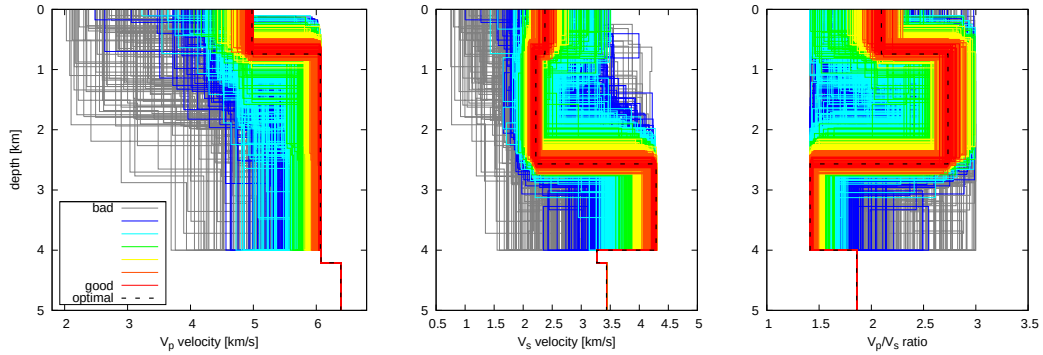

Station PYL (epicentral distance 170 km, azimuth 185°), misfit 0.58

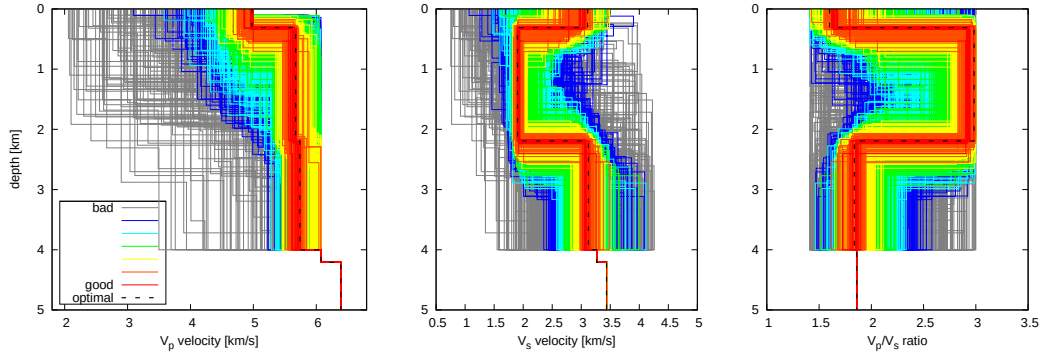

Figure 5.2: Results of the topmost crustal inversion of four single stations. All models, where the forward problem was solved, are shown, color scale being related to the misfit value. Best model is displayed by black dashed line, than decreasing quality is shown by rainbow spectrum from red (misfit less than 1.005 of best value) to blue (misfit 1.16–1.32 of best one) with exponentially increasing width of color sets (described in the text in detail). Models with misfit worse than 1.32 of best one are in gray. Shown below 4 km is the model of Table 5.1 kept fixed in this study.

Station EVR (epicentral distance 56 km, azimuth 351°), misfit 1.27

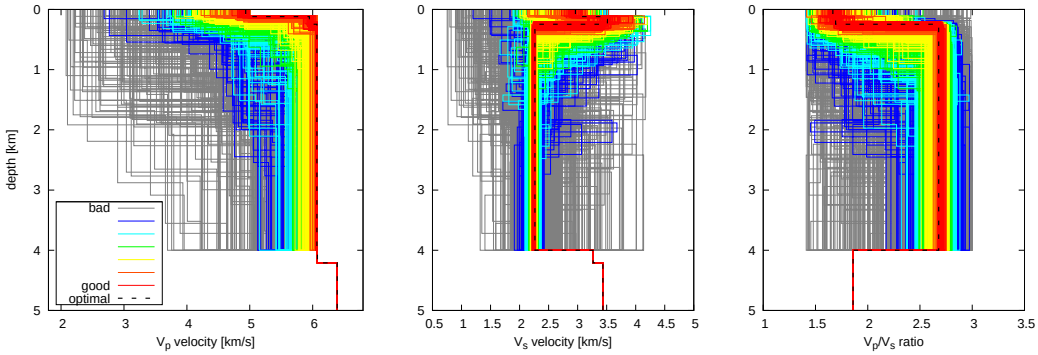

Station LTK (epicentral distance 102 km, azimuth 115°), misfit 0.52

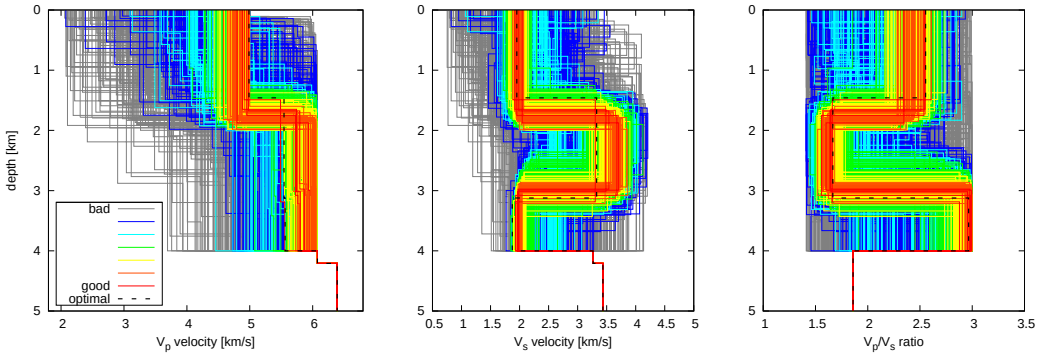

Station VLX (epicentral distance 123 km, azimuth 161°), misfit 0.81

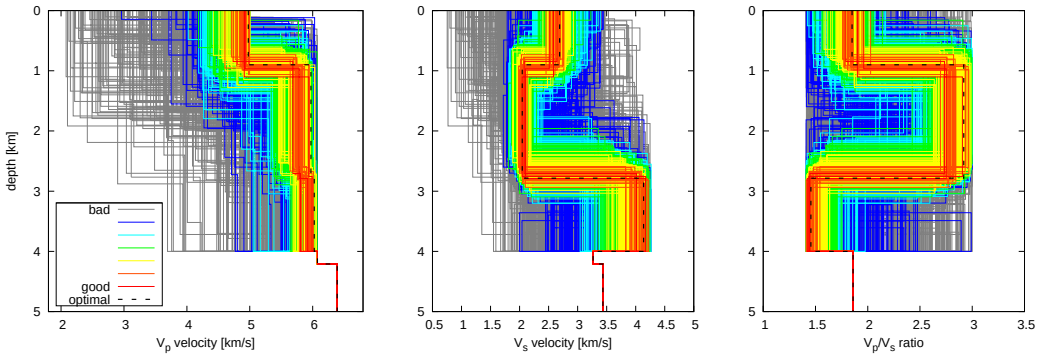

Station PYL (epicentral distance 170 km, azimuth 185°), misfit 0.62

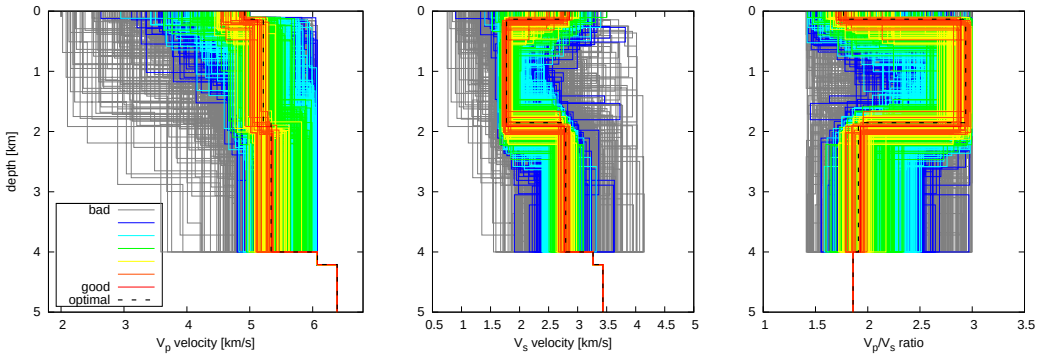

Figure 5.3: Results as in Fig. 5.2, but the 'trial source delay' feature (adjusting origin time to find best fit) was disabled.

Station EVR (epicentral distance 56 km, azimuth 351°), misfit 1.27

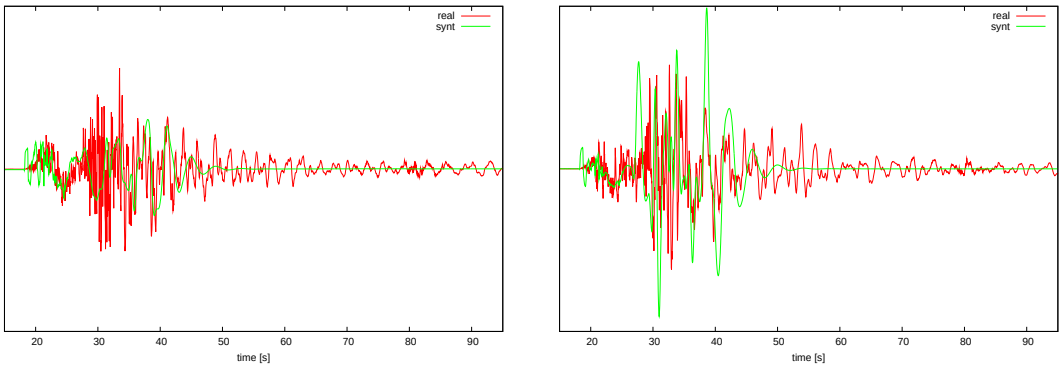

Station LTK (epicentral distance 102 km, azimuth 115°), misfit 0.52

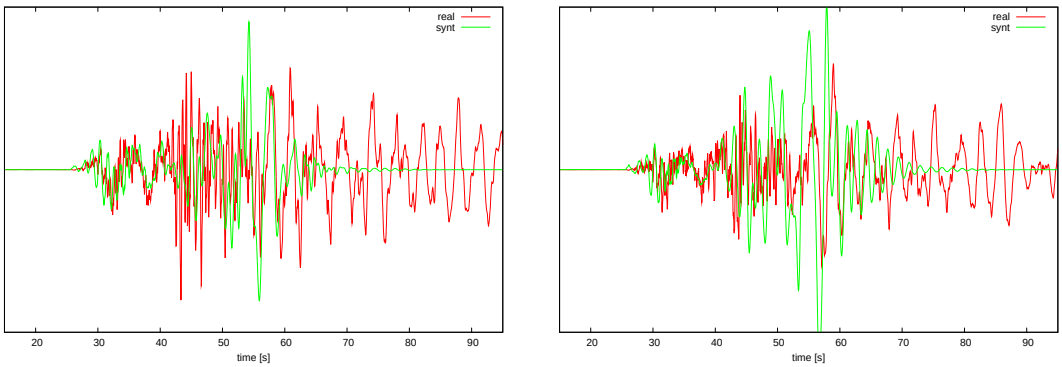

Station VLX (epicentral distance 123 km, azimuth 161°), misfit 0.81

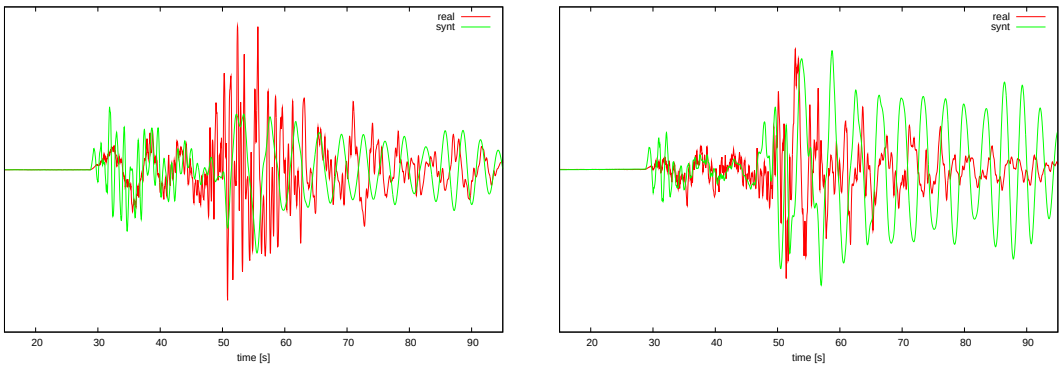

Station PYL (epicentral distance 170 km, azimuth 185°), misfit 0.62

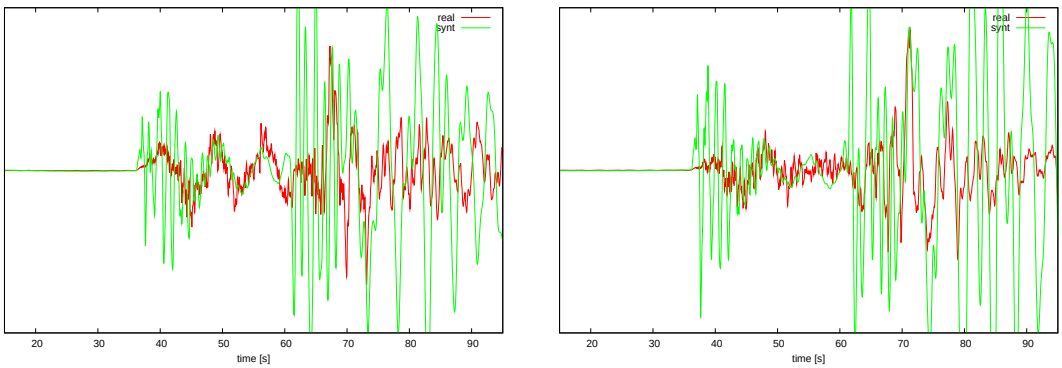

Figure 5.4: Comparison of the real records (red) and the best-fitting synthetics (green) calculated in the best models obtained by solving inverse problem (Fig. 5.3). Radial component is in the left panels, vertical in the right ones. Intention was to fit the FLP-wave between the P- and S-wave arrival. Notice that shown are seismograms up to 10 Hz, although they were compared up to 0.3 Hz while evaluation the misfit.

Stations EVR, LTK, VLX and PYL, misfit 1.33

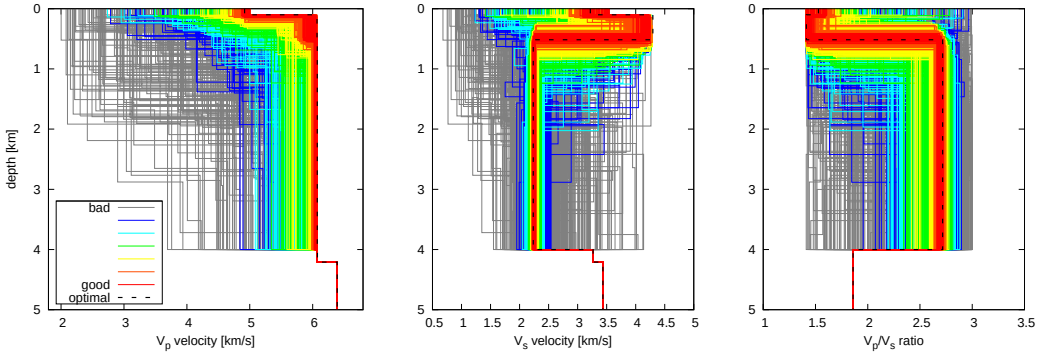

Figure 5.5: Models found by simultaneous inversion of 4 stations. The color palette is the same as in Fig. 5.2.

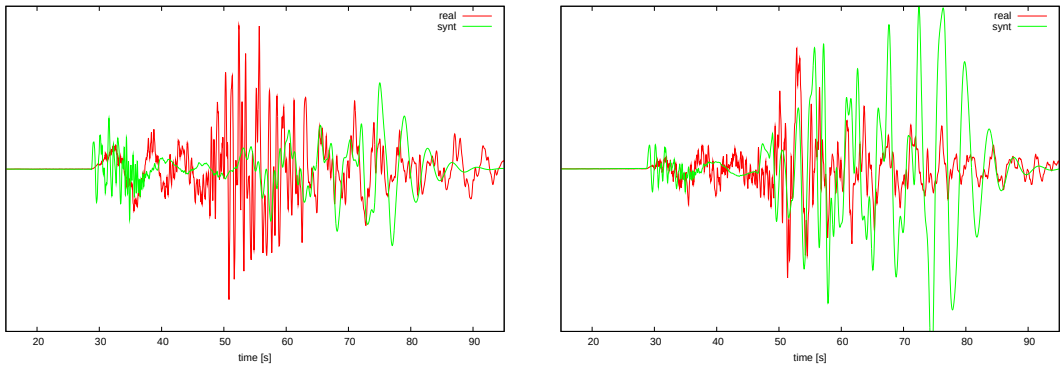

Figure 5.6: Comparison of the radial (left) and vertical (right) component of real record and synthetic at station VLX (epicentral distance 123 km, azimuth 161°). It was calculated in the 'best-fitting' model obtained by simultaneous inversion for 4 stations. Only the initial part of the FLP-wave is matched well.

joint inversion and plotted resultant model (Fig. 5.5). The synthetic seismograms in the best-fitting model contain the FLP-wave, but agree poorly with real ones (Fig. 5.6). The result is that the FLP-wave at these 4 stations cannot be well explained by a single 1-D crustal model. Nevertheless, a long period wave group in the initial part of record is present in the synthetics, and the model in Fig. 5.5 keeps the main features of the single-station models, mainly the large v_P/v_S ratio greater than 2.5 dominating in the studied 4-km zone.

So far, we have evaluated misfit by comparison of real and synthetic components N, E, Z. We tested whether the result changes if we rotate the records and compare only radial and vertical component, where the FLP-wave is significant. We used parametrization 'B' (Table 5.2), so we simultaneously tested parametrization with v_S low-velocity channel disabled. The trial source delay was disabled. The obtained models differ only slightly (see Fig. 5.7) and nearly no difference was observed between synthetic seismograms in both models (Fig. 5.8). It seems that it is not really important which components are compared while evaluating misfit function. The most important observation from this test is that a model without v_S low-velocity channel may be also successful.

Station PYL, misfit 0.83 (based on N, E, Z components)

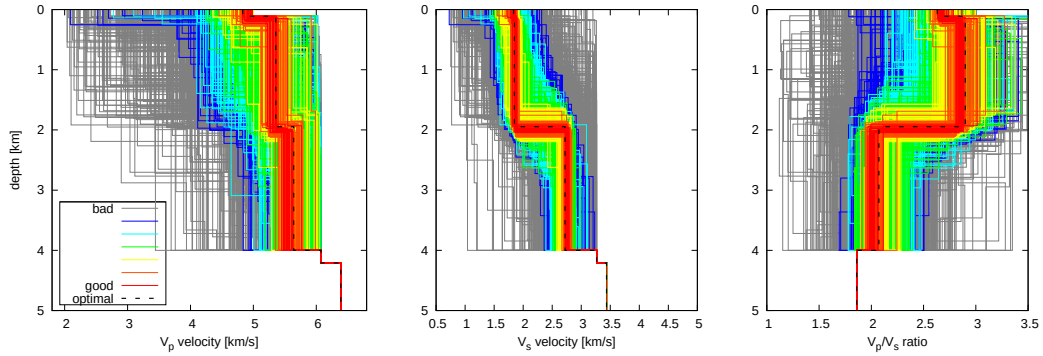

Station PYL, misfit 0.80 (based on R, Z components)

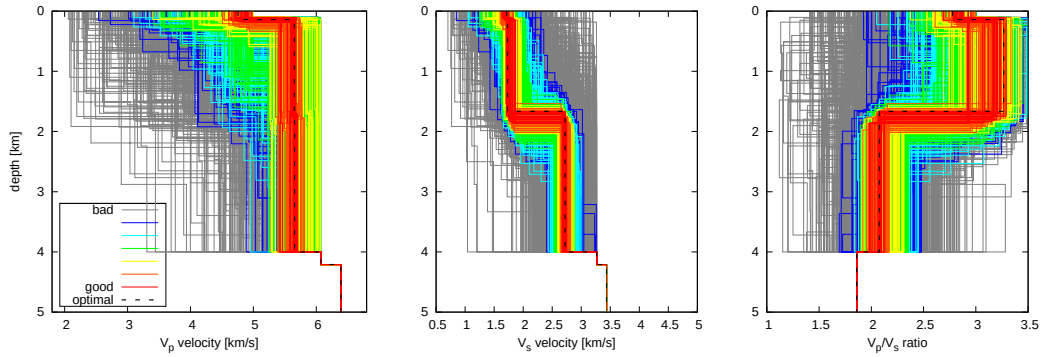

Figure 5.7: Comparison of the models obtained by solving inverse problem with misfit based on N, E, Z components (top) and R, Z components (bottom).

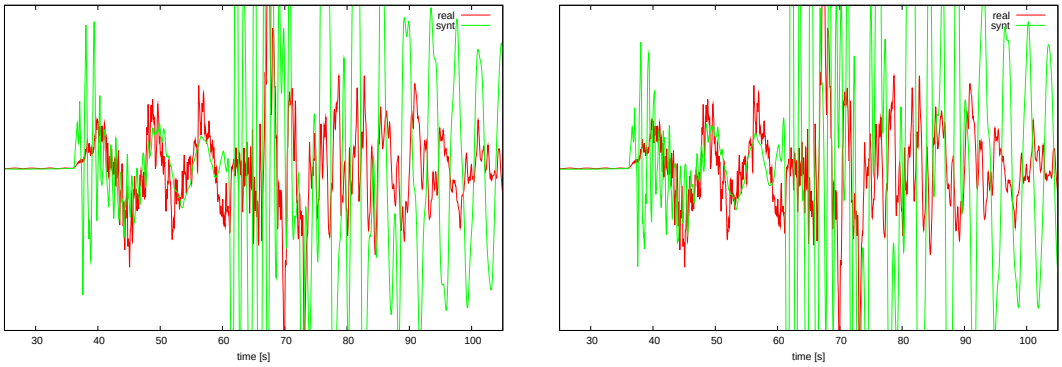

Figure 5.8: Comparison of the real records (red) and synthetics (green) calculated in models obtained by solving inverse problem with misfit based on comparison of different component (Fig. 5.7) (left is with misfit based on N, E, Z, right on R, Z). The synthetic records only slightly differ. Radial component at station PYL (epicentral distance 170 km, azimuth 185°) is displayed.

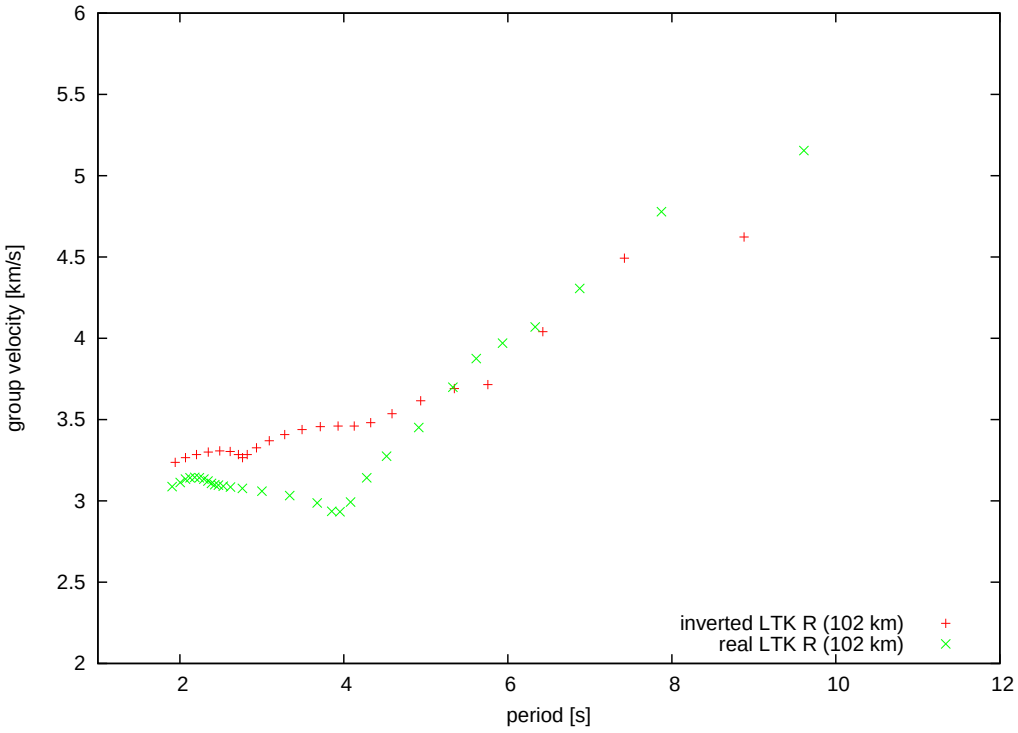

Figure 5.9: Comparison of the dispersion curve for the real data (green) and the curve obtained by dispersion analysis from synthetic seismogram in optimal model found by inversion (red). The analysis of the synthetics was exactly the same as if they were real data. Radial component of station LTK (Loutraki, epicentral distance 102 km) is plotted. The best agreement between the curves is in the period range 5–8 seconds, where there are the predominant periods of the FLP-wave.

5.4 Dispersion curve for the optimal model

We used the dispersion curves as an independent validation. We analyzed the synthetic seismograms provided by the best-fitting crustal models. We used SVAL program, all parameters of the frequency-time analysis were the same as in analysis of the real data. The obtained dispersion curve was compared to the corresponding curve for the real data at the same stations (Fig. 5.9).

Compared to real dispersion curves, we can see that the wave groups found in the synthetics were also dispersive, with similar characteristic as the real one, but the agreement between corresponding curves is not very good. The comparison supports the idea that the synthetic seismograms do contain the FLP wave, i.e. the modeled wave is of the same nature as the real one. When plotted into 'generalized dispersion curves' shown in Chapter 3, we found that some of the dispersion curves in inverted models belong to one of the 'strips', but not all, one station is systematically slower (Fig. 5.10).

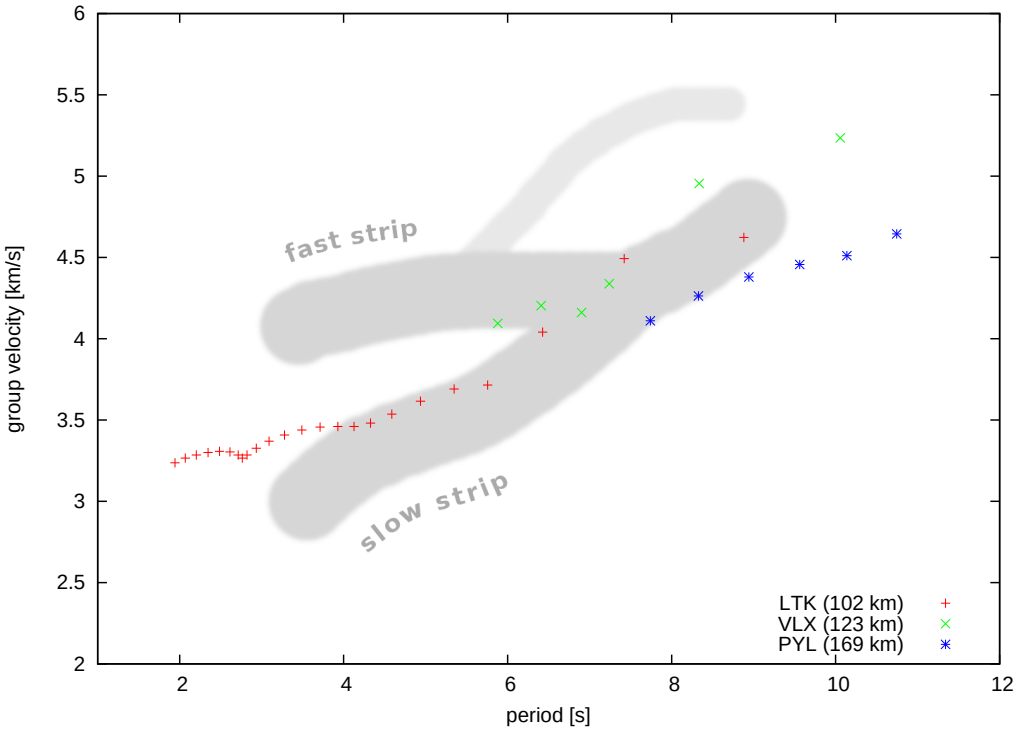

Figure 5.10: Dispersion curves of the FLP-wave obtained from analysis of synthetic seismograms in three different crustal models. The models were obtained by inversion of real seismograms at the three stations. The gray strips are generalized dispersion curves obtained from real data (Fig. 3.5).

6. Interpretation of FLP-wave

In this chapter, we will use findings from the previous chapters to look for theoretical explanation of the FLP-wave. Figuratively, pieces of mosaic from observation, data analysis, modeling and inversion join together to provide a suitable theory.

6.1 Analysis performed

The aim of this analysis is to find physical interpretation of optimal model in terms of higher modes, including leaking modes. First of all, a model with well-developed FLP-wave is required. We used one of the models obtained by inversion in Chapter 5, coming from station PYL. We altered it adding Mohorovičić discontinuity according to model *Novotny* (Novotný *et al.*, 2001). The resultant model, in which the following analysis was done, is shown in Fig. 6.1 and Table 6.1.

depth [km]	v_P [km/s]	v_S [km/s]	ρ [g/cm^3]	Q_P	Q_S
0.00	4.92	2.78	2.7	300	150
0.13	5.22	1.78	2.7	300	150
1.85	5.34	2.80	2.9	300	150
4.00	6.07	3.27	2.9	300	150
4.20	6.39	3.43	3.0	300	150
12.00	6.40	3.44	3.0	300	150
27.10	6.88	3.70	3.1	300	150
33.00	8.37	4.70	3.37	300	150

Table 6.1: Crustal model used in the comparison of dispersion curves of FLP-wave. It was obtained by inversion at station PYL, Mohorovičić discontinuity added according to model *Novotny*.

The purpose of next steps is to compare 'experimental' dispersion curves obtained by frequency-time analysis of synthetic seismograms with theoretical ones calculated from dispersion equation for Rayleigh wave higher modes and leaking modes.

We calculated synthetic seismograms (one of them shown in Fig. 6.2) and analyzed their radial components by the SVAL program in the same way, which

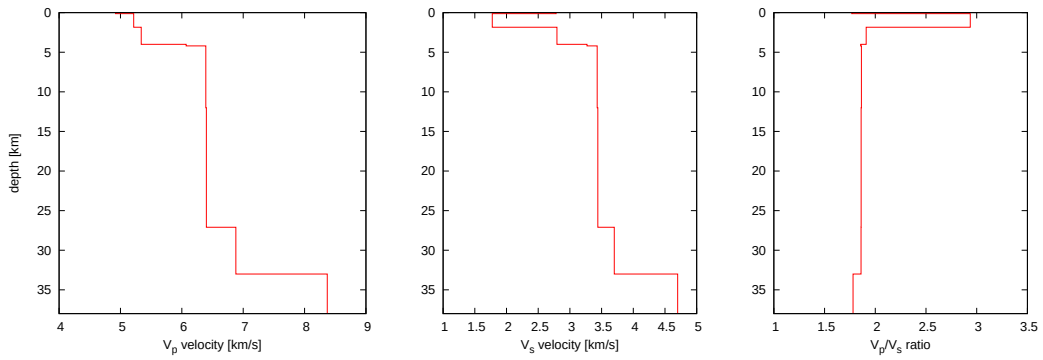

Figure 6.1: Model of Table 6.1.

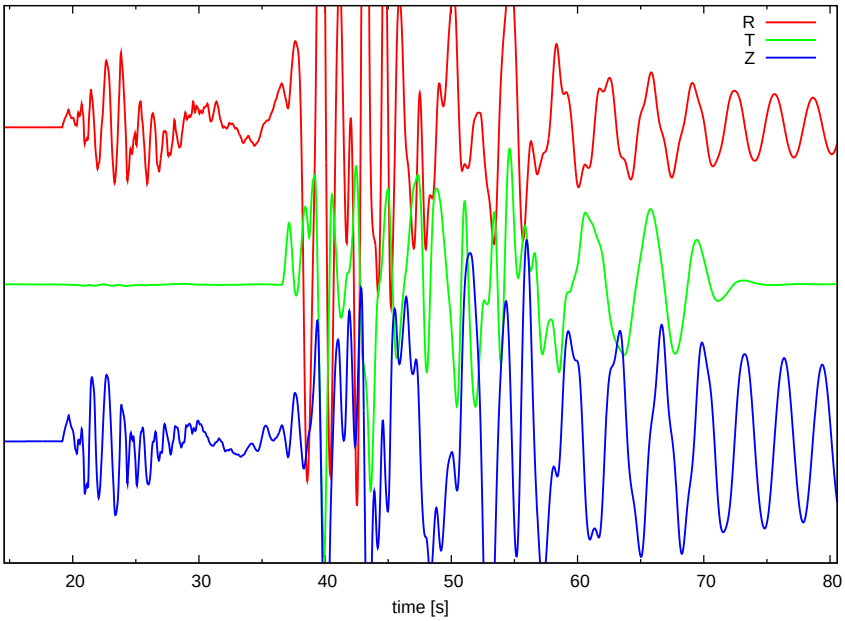

Figure 6.2: Synthetic seismogram at station VLX (Vlahokerasia, epicentral distance 123 km) with a strong FLP-wave, calculated in model coming from the inversion.

we used for the analysis of the real data in Chapter 3. We used dispersion curves from three stations where the FLP-wave was strong and well-fitted by the wave group corresponding to the selected dispersion curve in the SVAL (Fig. 6.3). The difference between curves in Fig. 6.4 (which should be theoretically the same, i.e. station independent) gives us an insight into its uncertainty.

Then we derived the theoretical dispersion curves by solving dispersion equation in program VDISP (described in section 2.3). In the first step, we calculated curves of the fundamental mode and four higher modes. In Fig. 6.4, they are compared to the points of 'experimental' dispersion curve from SVAL. It seems that a part of 'experimental' dispersion curve may be explained by the third higher mode of the Rayleigh wave. Nevertheless, the fastest velocities at periods longer than ~ 7.5 s are not matched.

The leaking-modes calculation requires a trick, because they correspond to complex roots of the dispersion equation which cannot be computed by VDISP program. The solution is to add an artificial jump to higher velocity under the deepest boundary of the model. After this formal step, leaking modes correspond to real roots (Oldřich Novotný, personal communication). In other words, the trick almost does not change the computed wave field. The seismograms and dispersion curves remain the same as in the medium without the artificial jump, including the leaking modes. However, using the trick, formal description of the wave field (in term of the dispersion equation) can be achieved with real roots. We added a half-space with $v_P = 9.0$ km/s and $v_S = 5.2$ km/s below the depth of 200 km.

The result is displayed in Fig. 6.5. The 'experimental' dispersion curve corresponds to the superposition of second, third and fourth leaking mode. Probably, these modes are close to each other so that they appear as a single wave in the seismograms.

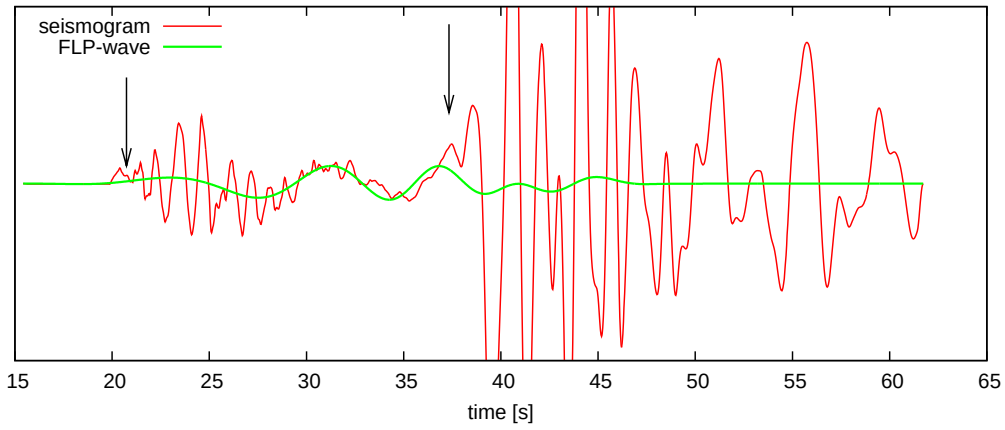

Figure 6.3: Confirmation that we have correctly chosen the FLP-wave (in SVAL program). The synthetic seismogram at station VLX (red) with a wave group corresponding to selected dispersion curve in the spectrogram (green). Black arrows mark the approximate arrival times of P-wave and S-wave.

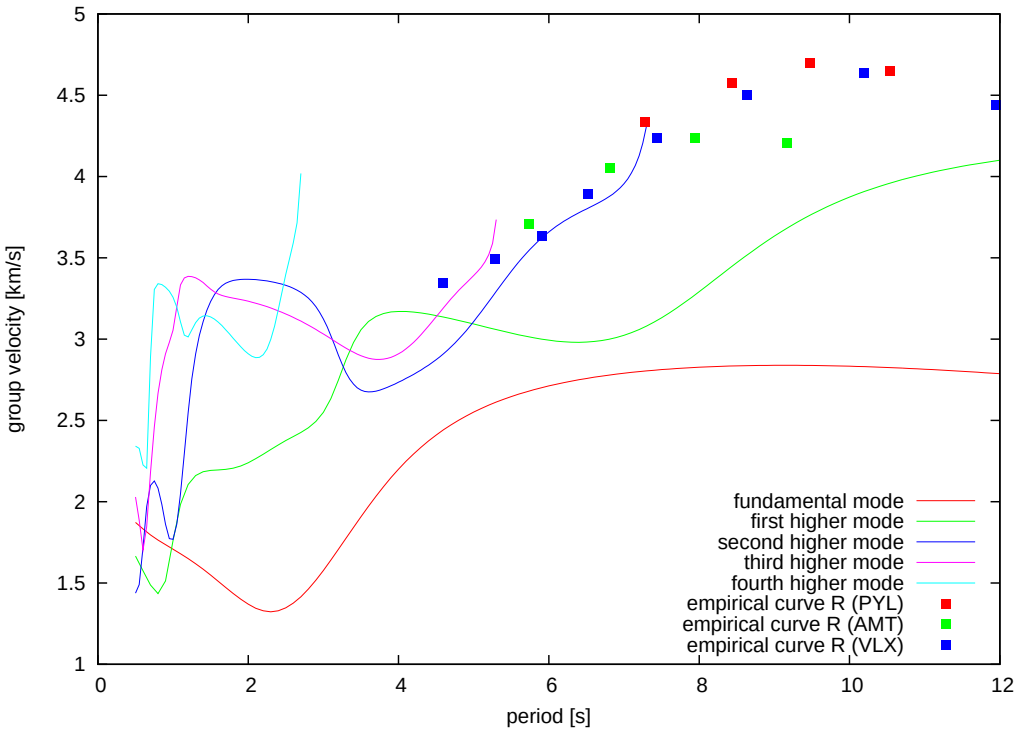

Figure 6.4: Theoretical dispersion curves calculated by VDISP for Rayleigh wave fundamental mode (red line) and four higher modes (the other color lines) compared to 'experimental' dispersion curves obtained by SVAL for synthetic seismograms in the same model (points).

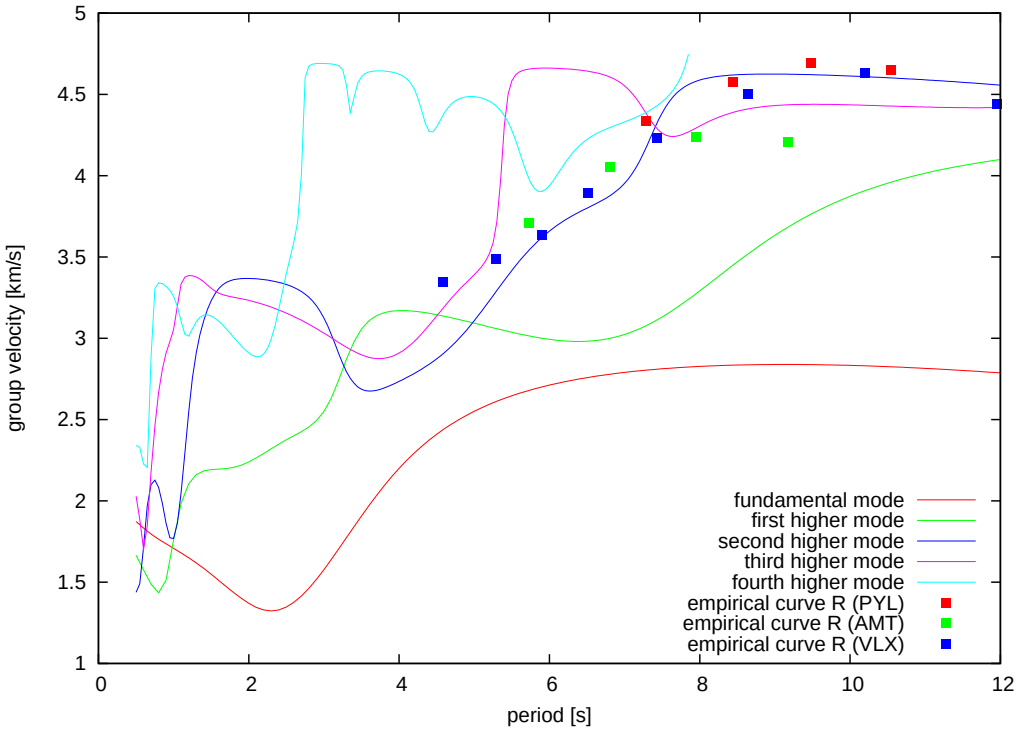

Figure 6.5: Theoretical dispersion curves similar to those in Fig. 6.4, but in model with high-velocity half-space added below 200 km depth – a 'tricky' way of calculation leaking modes. 'Experimental' dispersion curves obtained by SVAL using synthetic seismograms (points) corresponds to three different leaking modes (blue, magenta and azure line). Note that the experimental points are same as in Fig. 6.4, by now they are well matched by the calculated dispersion curves.

6.2 Discussion of results

We have found, that crustal model obtained by inversion agrees with observation in terms of FLP-wave properties and the FLP-wave can be explained as a superposition of higher leaking modes. The dispersion curve derived from synthetic seismogram by the methods of frequency-time analysis fits theoretical dispersion curves of several leaking modes calculated by solving dispersion equation of Rayleigh waves with a trick.

The main feature of the crustal models enabling explanation of the observed FLP-waves is a very high ratio $v_P/v_S > 2.5$. Bouchon (1981) mentioned importance of the high v_P/v_S ratio on the generation of the leaking modes.

It is to mention, that calculating leaking modes as normal modes in altered model is a kind of approximation, moreover requiring a guess of depth and velocity of the formally added layer. To be more certain about the results reliability, we tried to move the high-velocity half-space down to 500 km. Dispersion curves slightly changed, but the resultant conclusion about superposition of three leaking modes needed to fit the data remains the same.

The split of observed dispersion curves at shorter periods mentioned in Chapter 3 could be probably also explained by different leaking-mode branches, compare azure line in Fig. 6.5 and the upper strip in Fig. 3.5, but that question requires further investigation.

Conclusion

The unusual fast long-period (FLP) waves were found in records of the Efpalio 2010 earthquake. The waves were observed in the initial part of the record, in the interval between P- and S-wave arrival and have periods ranging from 4 to 8 seconds. After rotating the records into R, T, Z system by means of station azimuth the FLP-wave was found to be strong on the radial and vertical component but weak or absent on the transversal component. The latter suggests its relation to Rayleigh waves, while the large group velocity suggests relation to some higher modes. Therefore initially, the idea was to study dispersion of FLP-wave, both experimentally and theoretically. Experimental study means to use methods of the frequency-time analysis, theoretical study means finding relations to analytically derived dispersion curves of higher modes.

Before studying dispersion characteristics of the observed FLP-waves, we made tests to understand feasibility of the frequency-time analysis to obtain experimental dispersion curves. We performed synthetic tests in which the dispersion curve of Rayleigh wave in synthetic seismograms was compared with a theoretical dispersion curve. We found out that there are problems at near stations, probably caused by overlapping of the fundamental mode with some higher modes. The dispersion curves for more distant stations were much closer to the theoretical (distance independent) curve, but only in the period range prevailing in the Rayleigh wave. Specifically, for periods shorter than 2 s, and longer than 6 s, the 'experimental dispersion curve' (that from synthetic records) and the theoretical one differ significantly. This is an important warning that the dispersion curves coming from the frequency-time analysis should always be used with a great caution. Epicentral distances, predominant periods, hence also signal-to-noise ratio may have critical effects.

Despite the recognized problems we analyzed dispersion of the fast long-period (FLP) waves observed in real records of the Efpalio 2010 earthquake, using methods of the frequency-time analysis. The obtained dispersion curves featured large variations among the stations. We divided the curves into a few groups according the FLP-wave strength and evaluated the fit between the FLP wave and its approximation obtained by means of the dispersion analysis. The group of the reliable (well rated) dispersion curves split into 2 to 3 major strips (Fig. 3.5).

Split of the dispersion into the strips, together with some doubts about relevance of the dispersion curves, implied that the experimental dispersion curves do not represent suitable input data to be inverted for the crustal structure. Moreover, theoretical dispersion curves of standard modes, which we are able to calculate, do not help. It is so because we do not have a theoretical description of the FLP-wave. Therefore, in contrast to the initial idea (to model the dispersion curves) we decided to model directly seismograms, without an intermediate step via dispersion curves.

Observed seismograms of the FLP-waves were subjected to modeling. Syn-

thetic seismograms were calculated by the Discrete wavenumber method, using the previously found source position and focal mechanism. Forward simulations for several existing crustal models of the studied region were made, as well as for some altered models. None of the models produced as clear and strong FLP-waves as those observed. A few partially successful models served for a sensitivity study, which indicated that the FLP-wave is controlled by relatively shallow part at the top of the crust with depth less than 4 km. The velocity contrast on the bottom boundary of such a 'layer' is also important. This finding supports an idea, that the observed splitting of the dispersion curve into strips is related to lateral variations of the crustal structure.

To better understand the generation and propagation of the FLP-wave, the shallow upper-crustal structure (down to the depth of 4 km) was retrieved by inverting observed FLP-wave seismograms by means of the Neighborhood algorithm. Uncertainty of the model parameters (v_P, and v_S velocities, and the layer thicknesses) was examined, besides other by repeating the inversion with various constraints, e.g. enabling/disabling a local minimum of v_S, i.e. the low-velocity channel. We obtained well-fitting models for single stations. Their common feature is a zone of a high v_P/v_S ratio (> 2.5), see, e.g. Fig. 5.7. Future tests should validate how much this result might be affected by limited v_P resolution by the Rayleigh waves. No satisfactory model could be found when inverting stations simultaneously. Thus, the FLP-waves can be explained by a 1-D crustal model, but the model is path-dependent, i.e. no suitable 1D 'universal' model of the shallow structure exists for the whole studied region.

As an independent validation, we analyzed the synthetic seismograms provided by the best-fitting crustal models. We compared their dispersion curves with experimental dispersion curves (real data), both derived by the frequency-time analysis (Fig. 5.10). The wave group found in the synthetics was also dispersive, with similar characteristic as the real one. The comparison supports the idea that the best-fitting synthetic seismograms do contain the FLP wave.

Finally, theoretical dispersion curves in the model originated from the inversion have been derived for normal modes of Rayleigh wave, as well as for leaking modes. They were compared to the dispersion curve of the FLP-wave obtained by dispersion analysis of synthetic seismograms in the same best-fitting crustal model. It indicates that the FLP-wave corresponds to superposition of some higher leaking modes (Fig. 6.5). We have found not only an explanation for observed data in terms of suitable crustal model producing similar waves, but also in terms of theoretical description of the wave.

The conclusion from all methods which we used is that the observed FLP-wave is a dispersive wave of Rayleigh type, with interference character originating in near-surface (topmost 2–4 km) low-velocity layers of the crust. It can be explained as a superposition of higher leaking modes. Nevertheless, we believe that practical investigation of the wave is easier using complete synthetic seismograms (and/or their dispersion curves), rather than using theoretical dispersion curves of individual modes.

Being controlled by the relatively shallow structure, the FLP-wave appears to be a new powerful tool for the structural investigations, efficiently complementing methods in which the topmost crustal part is not properly addressed (such as, e.g. in the local-earthquake passive tomography). It remains to find out whether the FLP-wave might also have a potential to precise the earthquake location depth.

As an outlook, further modeling and analysis of another earthquake might help to find out whether the FLP-wave is controlled by a local structure around the station or by an 'average structure' of the path between epicenter and station. This question exceeds the scope of the thesis, but it is one of possible future research aims. The study of another earthquake will be also useful for validation of the results. An open question remains whether the FLP-waves exists in records of deeper crustal earthquakes (e.g. the source depth of about 20 km), and/or in another region. Completely out of scope is also geological interpretation of the successful crustal models which will definitely need a cooperation with a geology expert.

Bibliography

Bouchon M. (1981). A simple method to calculate Green's function for elastic layered media, *Bull. Seismol. Soc. Am.,* **71**, 959–971.

Dainty A. M. (1971). Leaking modes in a crust with a surface layer, *Bull. Seismol. Soc. Am.,* **64** (1), 93–107.

Gök R., R. J. Mellors, E. Sandvol, M. Pasyanos, T. Hauk, R. Takedatsu, G. Yetirmishli, U. Teoman, N. Turkelli, T. Godoladze and Z. Javakishvirli (2011). Lithospheric velocity structure of the Anatolian plateau-Caucasus-Caspian region, *J. Geophys. Res.,* **116**, B5, doi: 10.1029/2009JB000837.

Kanamori H. and L. Rivera (2008). Source inversion of W phase: speeding up seismic tsunami warning, *Geophys. J. Int.,* **175**, 222–238, doi: 10.1111/j.1365-246X.2008.03887.x.

Kennett B. L. N. and N. J. Kerry (1979). Seismic waves in a stratified half space, *Geophys. J. R. Astron. Soc.,* **57**, 557–583.

Kolínský P. (2004). Surface wave dispersion curves of Eurasian earthquakes: the SVAL program, *Acta Geodyn. Geomater.*, **1** (134), 165–185.

Kolínský P. (2010). *Surface Wave Analysis and Inversion, Application to the Bohemian Massif.* Praha. PhD. thesis. Faculty of Mathematics and Physics, Charles University Prague. Supervisor RNDr. Johana Brokešová, CSc. Available at: `http://www.irsm.cas.cz/~kolinsky/publications/thesis.pdf`.

Latorre D., J. Virieux, T. Monfret, V. Monteiller, T. Vanorio, J.-L. Got and H. Lyon-Caen (2004). A new seismic tomography of Aigion area (Gulf of Corinth, Greece) from the 1991 data set, *Geophys. J. Int.,* **159**, 1013–1031, doi: 10.1111/j.1365-246X.2004.02412.x.

Lee W. H. K. and C. M. Valdés (1989). User manual for HYPO71PC, Chapter 9, in Lee, W.H.K., ed., IASPEI Software Library Volume 1, Toolbox for seismic data acquisition, processing, and analysis: El Cerrito, Calif., International Association of Seismology and Physics of the Earth's Interior in collaboration with Seismological Society of America, p. 203-236.

Novotný O., J. Zahradník and G-A. Tselentis (2001). Northwestern Turkey earthquakes and the crustal structure inferred from surface waves observed in western Greece, *Bull. Seismol. Soc. Am.,* **91**, 875–879.

Novotný O., J. Janský, V. Plicka and H. Lyon-Caen (2008). A layered model of the upper crust in the Aigion region of Greece, inferred from arrival times of the 2001 earthquake sequence, *Stud. Geophys. Geod.,* **52**, 123–131.

Novotný O., E. Sokos and V. Plicka (2012). Upper crustal structure of the western Corinth gulf, Greece, inferred from arrival times of the January 2010 earthquake sequence, *Stud. Geophys. Geod.,* submitted.

Oliver J. (1961). On the long period character of shear waves, *Bull. Seismol. Soc. Am.,* **51** (1), 1–12.

Oliver J. and M. Major (1960). Leaking modes and the PL phase, *Bull. Seismol. Soc. Am.,* **50** (2), 165–180.

Proskuryakova T. A., O. Novotny and E. V. Voronina (1981). *Studies of the Earth's Structure by Surface Wave Method (Central Europe).* Nauka, Moscow, 96 pp. (in Russian).

Rigo A., H. Lyon-Caen, R. Armijo, A. Deschamps, D. Hatzfeld, K. Makropoulos, P. Papadimitriou and I. Kassaras (1996). A microseismic study in the western part of the Gulf of Corinth (Greece): implications for large scale normal faulting mechanisms, *Geophys. J. Int.,* **126**, 663–688.

Sambridge M. (1999). Geophysical inversion with a neighbourhood algorithm – I. Searching a parameter space, *Geophys. J. Int.,* **138** (2), 479–494, doi: 10.1046/j.1365-246X.1999.00876.x.

Sokos E., J. Zahradník, A. Kiratzi, J. Janský, F. Gallovič, O. Novotný, J. Kostelecký, A. Serpetsidaki and G.-A. Tselentis (2012). The January 2010 Efpalio earthquake sequence in the western Corinth Gulf (Greece). *Tectonophysics,* doi: 10.1016/j.tecto.2012.01.005.

Su S. and J. Dorman (1965). The use of leaking modes in seismogram interpretation and in studies of crust-mantle structure, *Bull. Seismol. Soc. Am.,* **55** (6), 989–1021.

List of Tables

List of Abbreviations

FLP-wave
fast long-period wave

DW method
Discrete wavenumber method

NA
Neighborhood algorithm